https://doi.org/10.5194/angeo-2020-9
Preprint. Discussion started: 31 March 2020

Annales Geophysicae Discussions
Open Access
EGU

A deep insight into the Ion Foreshock with the help of Test-particles Two-dimensional simulations

Philippe Savoini[1] and Bertrand Lembege[2]

[1]LPP (Laboratoire de Physique des Plasmas), Ecole Polytechnique, Route de Saclay, 91128, Palaiseau, France
[2]LATMOS (Laboratoire Atmosphères, Milieux, Observations Spatiales, IPSL/CNRS/UVSQ, 11 Bd d'Alembert, 78280, Guyancourt, France

Correspondence: P. Savoini (philippe.savoini@sorbonne-universite.fr)

Abstract. Two dimensional test-particles simulations based on shock profiles issued from 2D full PIC simulations are used in order to analyze the formation processes of ions backstreaming within the upstream region after these interact with a quasi-perpendicular curved shock front. Two different types of simulations have been performed based on (i) a "*FCE*" (Full Consistent Expansion) model which includes all self-consistent shock profiles at different times, and (ii) a "*HE*" (Homothetic Expansion) model where shock profiles are fixed at certain times and artificially expanded in space. The comparison of both configurations allows to analyze the impact of the front non stationarity on the backstreaming population. Moreover, the role of the space charge electric field is analyzed by switching it in/off in the simulations. A detailled comparison of these two last different configurations allows to show that the electric field component plays a key role in the ion reflection process within the whole quasi-perpendicular propagation range. Simulations evidence that the different populations observed *in-situ* namely the "*FAB*" (Field-Aligned Beam) and "*GBP*" (Gyro-Phase Bunch) populations are essentially formed by a $\overrightarrow{E}_t \times \overrightarrow{B}$ drift involving the convective electric field $\overrightarrow{E}_t$. Simultaneously, the study emphasizes the leading role of the electrostatic (longitudinal) field $\overrightarrow{E}_l$ built up within the shock front in the acceleration process in addition to the magnetic mirror reflection (Fast Fermi). This electrostatic field component appears as essential to form backstreaming ions at high θ_{Bn} angles and in particular at the edge of the ion foreshock around 70°. Moreover, the "*HE*" model shows that the rate $BI_{\%}$ of reflected ions is strongly dependent on the shock front profile which varies because of the shock front non stationarity. In particular, reflected ions appear to escape periodically from the shock front as "bursts" with an occurrence time period associated to the self-reformation of the shock front.

1 Introduction

While upstream ions interact with the curved terrestrial bow shock, a certain percentage is reinjected back into the solar wind and propagates along the interplanetary magnetic field (*IMF*): they form the so-called ion foreshock. This population has been extensively studied both with the help of experimental data (Tsurutani and Rodriguez, 1981; Paschmann et al., 1981; Bonifazi

https://doi.org/10.5194/angeo-2020-9
Preprint. Discussion started: 31 March 2020

Annales Geophysicae Discussions

and Moreno, 1981a, b; Fuselier, 1995; Eastwood et al., 2005; Oka et al., 2005; Kucharek, 2008; Hartinger et al., 2013) and numerical simulations (Blanco-Cano et al., 2009; Lembege et al., 2004; Savoini et al., 2013; Kempf et al., 2015; Savoini and Lembège, 2015).

Even if we restrict ourselves to the quasi-perpendicular region (i.e. for $45^o \leq \theta_{Bn} \leq 90^o$, where θ_{Bn} is the angle between the shock normal and the *IMF*), different types of backstreaming ions are observed: (a) some are characterized by a gyrotropic velocity distribution and form the field-aligned ion beam population (hereafter "*FAB*"), and conversely (b) others exhibit a non-gyrotropic velocity distribution and form the gyro-phase bunched ion population (hereafter "*GPB*"). None of these populations has yet a well established origin and different mechanisms have been proposed for years (Möbius et al., 2001; Kucharek et al., 2004): *(i)* scenarii based on the specular reflection (Sonnerup, 1969; Paschmann et al., 1980; Schwartz et al., 1983; Schwartz and Burgess, 1984; Gosling et al., 1982) with or without the conservation of the magnetic moment, *(ii)* scenarii which invoke the leakage of some magnetosheath ions producing low energy *FAB* population (Edmiston et al., 1982; Tanaka et al., 1983; Thomsen et al., 1983). Nevertheless, the origin of "*FAB*" ions could be due to *(iii)* the diffusion of some reflected ions (called "*gyrating ions*" because they are reflected by the supercritical shock front but do not manage to escape into the upstream region and go into the downstream region after their initial gyration (Schwartz et al., 1983)), by upstream magnetic fluctuations (Giacalone et al., 1994) or *(iv)* more directly by the shock ramp itself (with a pitch angle scattering during the reflection process) (Kucharek et al., 2004; Bale et al., 2005). All scenarii have some drawbacks and are not able to explain clearly the origin of both populations. On the other hand, "*GPB*" are preferentially observed at some distances from the curved shock front (Thomsen et al., 1985; Fuselier et al., 1986a) and their synchronized nongyrotropic distribution comes as part of a low-frequency monochromatic waves trapping (Mazelle et al., 2003; Hamza et al., 2006), or of beam-plasma instabilities (Hoshino and Terasawa, 1985). As a conclusion, it is quite difficult to discriminate between these different scenarii which can be present simultaneously or separately in time.

Our previous papers (Savoini et al., 2013; Savoini and Lembège, 2015) were focused on the origin of these two populations. Large scale two-dimensional PIC simulation of a curved shock has been used, where full curvature and time-of-flight effects for both electrons and ions are self-consistently included. Our simulations have shown that both "FAB" and "GPB" populations and their typical associated pitch angle distributions observed experimentally (Fuselier et al., 1986b; Meziane, 2005) have been retrieved not far from the front (until to 2 R_e). Moreover, results have shown that these two populations can be generated directly by the macroscopic E and B fields at the shock front itself. In other words, the differences observed between "*FAB*" and "*GPB*" populations are not the result of distinct reflection processes but are the consequence of the time history of ions interacting with the shock front: "*FAB*" population looses their initial phase coherency by suffering several bounces, in contrast with the "*GPB*" population which suffer mainly one bounce (Fermi type reflection process). This important result was not expected and greatly simplifies the question on each population origin (Savoini and Lembège, 2015)

Nevertheless, some further questions still need to be answered which are difficult to investigate with full PIC simulations (because of the self-consistency) in order to analyze several aspects of the reflection process. For this reason, we use herein complementary test-particle simulations to clarify the respective impact of the shock curvature and the time variation of the

https://doi.org/10.5194/angeo-2020-9
Preprint. Discussion started: 31 March 2020

Annales Geophysicae Discussions

macroscopic fields at the front on the back streaming ion reflection process. Then, the main questions presently addressed are summarized as follows:

1. Is the reflection process non-continuous in time (burst-type reflection process) or not ? In this case, how is it linked to the θ_{Bn} angle variation (i.e., space dependence) and/or to the shock profile variation (i.e. time dependence) ?

2. What is the impact of the space charge electric field localized within the shock ramp on the reflection process ?

3. What kind of reflection mechanisms can be identified in present simulations ?

The paper is organized as follows. Section 2 briefly summarizes the conditions of the previous 2D PIC simulations of the curved quasi-perpendicular supercritical shock and its associated ion foreshock obtained in Savoini and Lembège (2015). In section 3, results of test particles are presented and the ion reflection processes are investigated. Discussion and conclusions will be presented in section 4.

2 Numerical simulation conditions

The numerical conditions concerned in the present paper are similar to those described in Savoini et al. (2013) and Savoini and Lembège (2015). In short, we used a 2D dimensional, fully electromagnetic, relativistic particle code based on standard finite-size particle techniques (similar to Lembege and Savoini (1992, 2002) for planar shocks).

2.1 Self-consistent full PIC Simulations

The code solves Maxwell's equations in the Fourier space (so called pseudo-spectral technic) and then, fields are separated into transverse electromagnetic components (induced electric field), hereafter denoted by a subscript "t", and longitudinal electrostatic components hereafter denoted by a subscript "l" (space charge effects). The longitudinal components are essentially built up within the shock front due to the different dynamics of the ions and electrons, whereas the induced components are generated by the solar wind itself through the $\overrightarrow{E}_t = -\overrightarrow{U} \times \overrightarrow{B}$ term at the shock (where $\overrightarrow{U}$ is the bulk Solar Wind velocity).

In our configuration, the magnetostatic field is partially lying outside the simulation plane (see Savoini and Lembège (2001) for more details). Then, the simulation is limited to the whole quasi-perpendicular domain of shock propagation (i.e., for $45° \leq \theta_{Bn} \leq 90°$). We use a magnetic piston whose geometry is adapted to initiate a shock front with a curvature radius large enough as compared with the upstream ion Larmor gyroradius (R_c). This curvature increases to the end of the simulation. This configuration has two different consequences: (i) first, as θ_{Bn} decreases from $90°$, the shock front velocity slightly decreases, and so does the Alfvèn Mach Number M_A from ≈ 5 to ≈ 3, where the velocity is measured at $\theta_{Bn} = 90°$ used as a reference angle; (ii) the "time-of-flight" effects are self-consistently included. Indeed, this ballistic process is observed when the upstream magnetic field lines are convected by the incoming solar wind. In present simulations (based on upstream rest frame), the curved shock front expands and scans different θ_{Bn} values. As a result, backstreaming particles, collected at a given upstream location, come from different parts of the curved shock front depending on their respective velocity.

https://doi.org/10.5194/angeo-2020-9
Preprint. Discussion started: 31 March 2020

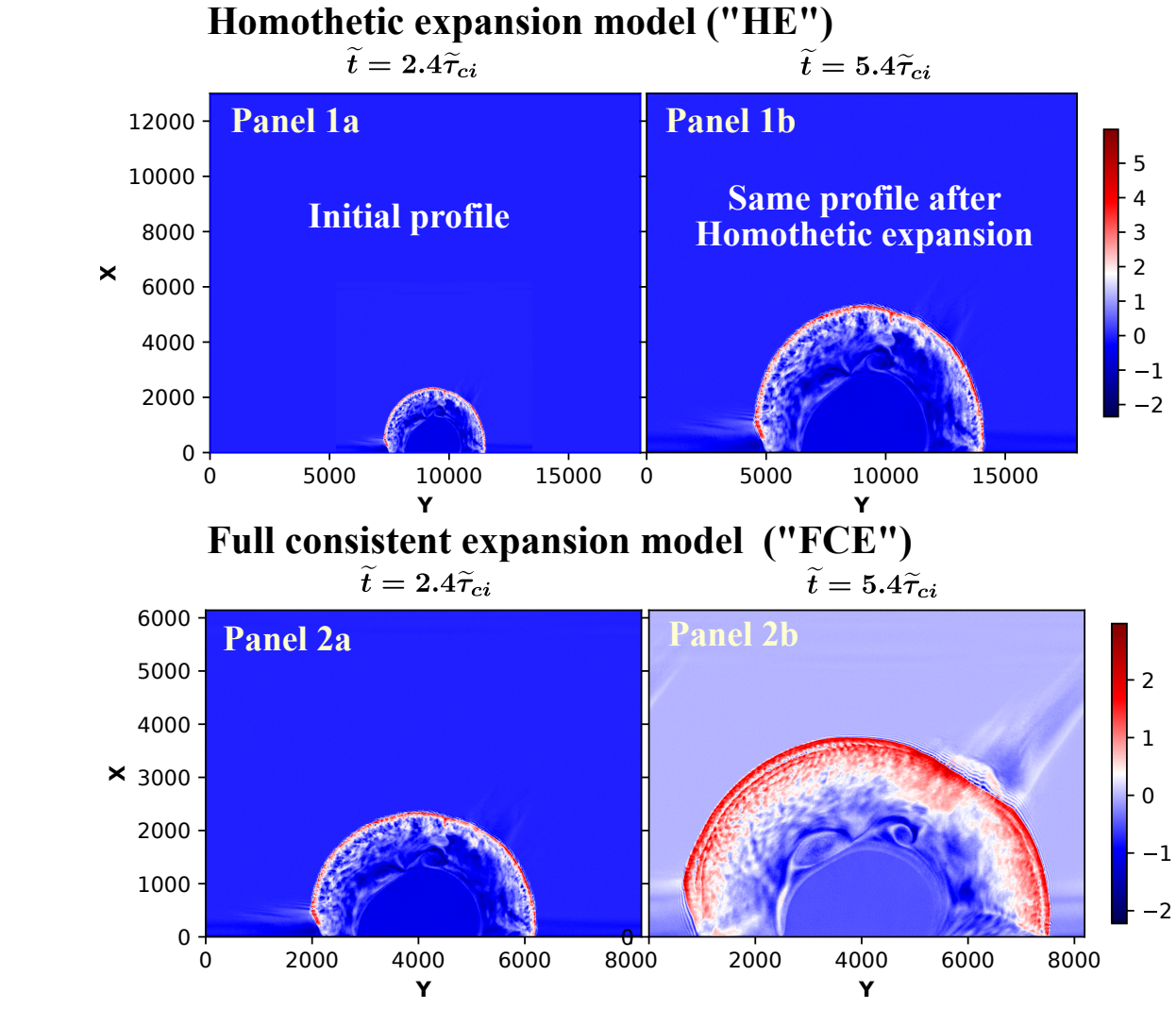

Figure 1. Panels 1a-b illustrate one example of the curved magnetic field $\widetilde{B}_{tz}$ in the homothetic expansion model "*HE*" (time independant), where the shock profile is fixed in time but expands in space via an expanding factor proportional to the shock front velocity $v_{shock}t$ (this shock profile has been chosen at time $\widetilde{t}_{init} = 2.4\widetilde{\tau}_{ci}$ of the self-consistent simulation). At this time, the shock wave dilates by a factor of 2.6 compared to its initial shape. In contrast, panels 1c-1d illustrate the evolution of the magnetic field $\widetilde{B}_{tz}$ in full consistent expansion model "*FCE*" (time dependant) simulation plotted after the same time evolution from $\widetilde{t}_{init} = 2.4\widetilde{\tau}_{ci}$ and $\widetilde{t}_{simul} = 5.4\widetilde{\tau}_{ci}$

.

https://doi.org/10.5194/angeo-2020-9
Preprint. Discussion started: 31 March 2020

Annales Geophysicae Discussions

Initial plasma conditions are summarized as follows: light velocity $\widetilde{c} = 3$, temperature ratio between ion and electron population $T_{el}/T_{io} = 1.58$. A mass ratio $m_i/m_e = 84$ is used in order to save CPU time and the Alfvèn velocity is $\widetilde{v}_A = 0.16$. The shock is in supercritical regime with a time averaged Alfvèn Mach number $M_A \approx 4$ measured at $\theta_{Bn} = 90°$. In order to observe the early stage of the ion foreshock formation, the end time of the simulation is $\widetilde{t}_{simul} = 5.4\widetilde{\tau}_{ci}$, which is large enough to investigate the interaction of incoming ions with the shock front and the further formation of back streaming ions.

2.2 Test particle simulations

In the present paper, we use all field components issued from the same previous PIC simulation as in Savoini and Lembège (2015); all components have been saved every $\Delta\widetilde{T} = \widetilde{\tau}_{ci}/20$. Test-particle simulations reveal to be a straightforward way to evaluate the action of different field components on the ion dynamics. Indeed, the feedback effects of particles on electromagnetic fields are excluded in test particle simulations, and one can modify or cancel some field components independently one from each other. This allows to identify their specific actions on particles and on the resulting ion reflection processes.

Figure 1 plots an example of the two configurations used hereafter in this paper. Panels 1a and 1b show one example of a so-called "homothetic" approach on the $\widetilde{B}_{tz}$ components at the selected time ($\widetilde{t}_{selected} = 2.4\widetilde{\tau}_{ci}$) till $\widetilde{t}_{end} = 5.4\widetilde{\tau}_{ci}$ when all test particles released in front of the shock wave have interacted with the front and leave it. In this particular approach named ***H**omothetic **E**xpansion" model* (hereafter named "*HE*"), particles move in a propagating "fixed front profile" i.e., all-time variations are excluded; only spatial inhomogeneities of the shock front profile chosen at the selected time are included, as detailed in Section 4. This model is in contrast with the ***F**ull **C**onsistent **E**xpansion model* (hereafter named *FCE*) illustrated in panels 2a-2b, which corresponds to results where test ions interact with the E and B fields issued from the self-consistent simulation and where both spatial inhomogeneities and nonstationarities are fully included.

In the two configurations "*HE*" and "*FCE*", we inject test particles distributed within 10 individual sampling boxes located along the curved shock front (Figure 2). This procedure allows us to analyze the impact of the front curvature (local θ_{Bn}) on the formation of backstreaming ions. We follow 1 million test particles. Then, each box has the same number of particles $N = 100000$ and are initialized as a Maxwellian distribution with a thermal velocity v_{thi} which is the same as in the self-consistent simulation (Savoini and Lembège, 2015).

For reasons of clarity, we have associated a different color to each box and all ions belonging to a given box have the same color.

Let us point out that the use of finite size sampling box at different initial θ_{Bn} angles does only estimate the location where the particles hit the shock but does not provide an exact value for the local θ_{Bn} finally seen by the particles when these interact with the expanding shock front. Nevertheless, it reveals to be quite helpful when classifying the different types of particle interactions with the curved front. The sizes of the box are chosen so that (i) along the curved shock front, each box has an angular extension of $\approx 4^o$ which is small enough to scan the different orientations of θ_{Bn} and large enough for statistical constraints, and (ii) along the local shock front normal where each box has a length large enough ($L_{size} = 2000\Delta x$) to ensure that most particles interact with the shock front during a noticeable time range (i.e., $D_T \approx 3\widetilde{\tau}_{ci}$).

Let us describe the "*HE*" expansion model (i.e. homothetic simulation approach) in more details.

https://doi.org/10.5194/angeo-2020-9
Preprint. Discussion started: 31 March 2020

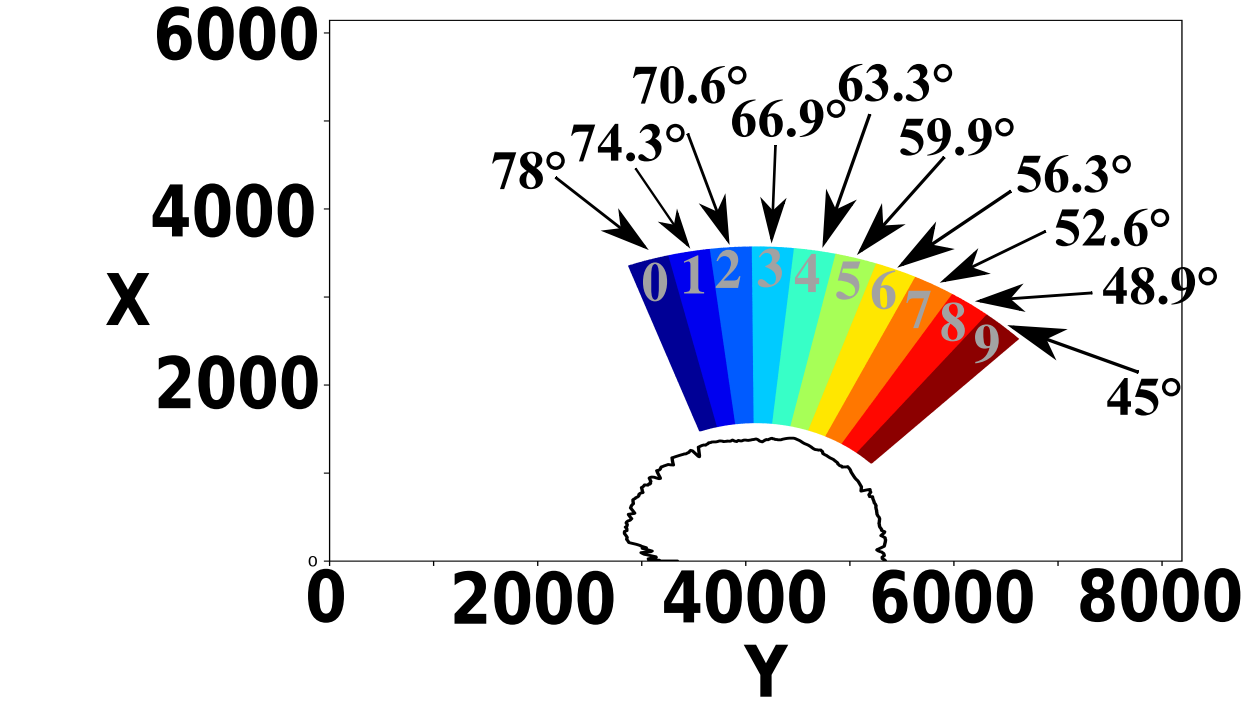

Figure 2. Initial position of the 10 sampling boxes which map the upstream ion foreshock region; all ions belonging to a given box are represented by the same color. The θ_{Bn} angle of propagation where each box is initially centered at time t= 0 is reported above the corresponding identification number of the box.

It is important to emphasize that all simulations are made in the Solar Wind reference frame (i.e., the curved shock expands into the "upstream region" where the Solar Wind is at rest). As a consequence, if one follows test particles within this configuration, we have to mimic this behavior. In order to proceed, we apply an homothetic transformation (homogeneous dilatation in all directions) with an expansion factor deduced from the shock front velocity determined at the selected time as illustrated in Panels 1a-b of Figure 1. Special attention has been taken in the determination of this homothetic factor $\lambda = v_{shock} * t$ in order to include an exact induced/convective electric field $\widetilde{E}_t$ (due to the relative motion between the Solar Wind and the shock front). In other words, all points of electromagnetic fields at the shock front follow the relation $\overrightarrow{OM} \longmapsto (v_{shock} * t)\overrightarrow{OM}$ where v_{shock} is the value of the shock velocity as computed from our self-consistent 2D PIC simulations at the selected time t and $\overrightarrow{OM}$ is the vector between the initial position of the shock front and any point of the field array. Then, the same procedure is repeated for another selected time, so that one can analyze the impact of different shock front inhomogeneities and curvature on ion dynamics; let us note that time of flight effects are always included. Then, each front profile is selected within a same simulation time range $D_T \approx 4\widetilde{\tau}_{ci}$. In summary, similar simulations are performed for 174 different times in order to simulate all the different shock profiles provided by the 2D PIC self-consistent simulation from $\widetilde{t}_{init} = 1.2\widetilde{\tau}_{ci}$ to $\widetilde{t}_{simul} = 5.4\widetilde{\tau}_{ci}$.

https://doi.org/10.5194/angeo-2020-9
Preprint. Discussion started: 31 March 2020

Annales Geophysicae Discussions

3 Numerical results: the Full Consistent Expansion Model "*FCE*"

For clarifying the presentation, we will split this section into two parts where we analyze respectively (i) the dynamics of the backstreaming ions in the different boxes and their main features in terms of spatial and time evolution, and (ii) their behavior when some field components are artificially excluded in the shock front.

3.1 General features of the backstreaming ions

Figure 3 plots the spatial distribution of backstreaming ions density for the different sampling boxes (defined in Figure 2) at the end time of the simulation for the "*FCE*" model. Different informations can be summarized as follows:

(i) The percentage of the backstreaming ions increases when moving further into the foreshock (i.e. for decreasing θ_{Bn}) from $BI_{\%} = 0.1$ for box $N_{Box} = 0$ to $BI_{\%} \approx 14$ for box $N_{Box} = 9$. This behavior is in agreement with previous experimental observations (Ipavich et al. (1981); Eastwood et al. (2005); Mazelle et al. (2005); Turner et al. (2014) and numerical simulations (Savoini and Lembège, 2015; Kempf et al., 2015). Even if this percentage is slightly higher than in previous hybrid simulation observations (which is around 4% (Scholer et al., 1993)), the variation of $BI_{\%}$ versus the propagation angle θ_{Bn} is well retrieved.

(ii) The upstream edge of the ion foreshock (dashed line in Figure 3 for $N_{Box} = 1$ or 10) is not parallel to the IMF but is the result of the "time-of-flight" effect included in our simulations (Savoini et al., 2013). At the end of the simulation, this edge starts from the shock at the same critical angle so called $\theta_{io,fore} \approx 66^o$, as found in our previous self-consistent simulations (Savoini et al., 2013; Savoini and Lembège, 2015).

(iii) We observe that the backstreaming ion density is not uniform along the shock normal but exhibits different maxima. Not only the spatial distribution is not the same for all boxes but is even not uniform within a given same box, i.e. backstreaming ions do not escape uniformly away from or along the shock front. For instance, boxes $N_{box} = 0 - 3$ evidence two distinct "spots" near the shock front indicated by black arrows. As θ_{Bn} decreases (i.e. $N_{box} = 5 - 9$) the right-hand "spot" disappears and backstreaming population increasingly aligns along the upstream magnetic field. Accordingly, the width of the reflection area (i.e. the width of the ion foreshock very near the shock front) shrinks from $\approx 50\rho_{ci}$ (for $N_{Box} = 0$) to $\approx 17\rho_{ci}$ (for $N_{Box} = 9$).

These two distinct "spots" may be explained by the different time histories of the backstreaming ions within the shock front as reported in Savoini and Lembège (2015). Actually, the interaction time strongly differs from one ion to another depending of its gyrating feature when it hits the shock front for the first time. Short and long interactions time can be defined depending whether the reflection process is respectively associated to a short or long displacement of the ion along the shock front before escaping upstream. If the individual trajectory of the reflected ions had been already evidenced in Savoini and Lembège (2015), present test-particle simulations allow to generalize the results via a statistical approach versus their initial position in the Solar Wind (i.e. versus the N_{box} parameter). Figure 4 plots the distribution of θ_{Bn} angle seen by the particles when these hit for the first time the shock front (hereafter named θ_{Bn}^{hit} in red color) and when they finally exit the shock front to escape upstream (hereafter named θ_{Bn}^{exit} in blue color). These statistical results are obtained by computing these angles for each particle. As a

https://doi.org/10.5194/angeo-2020-9
Preprint. Discussion started: 31 March 2020

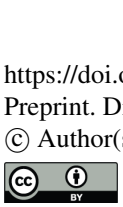

Annales Geophysicae Discussions
Open Access
EGU

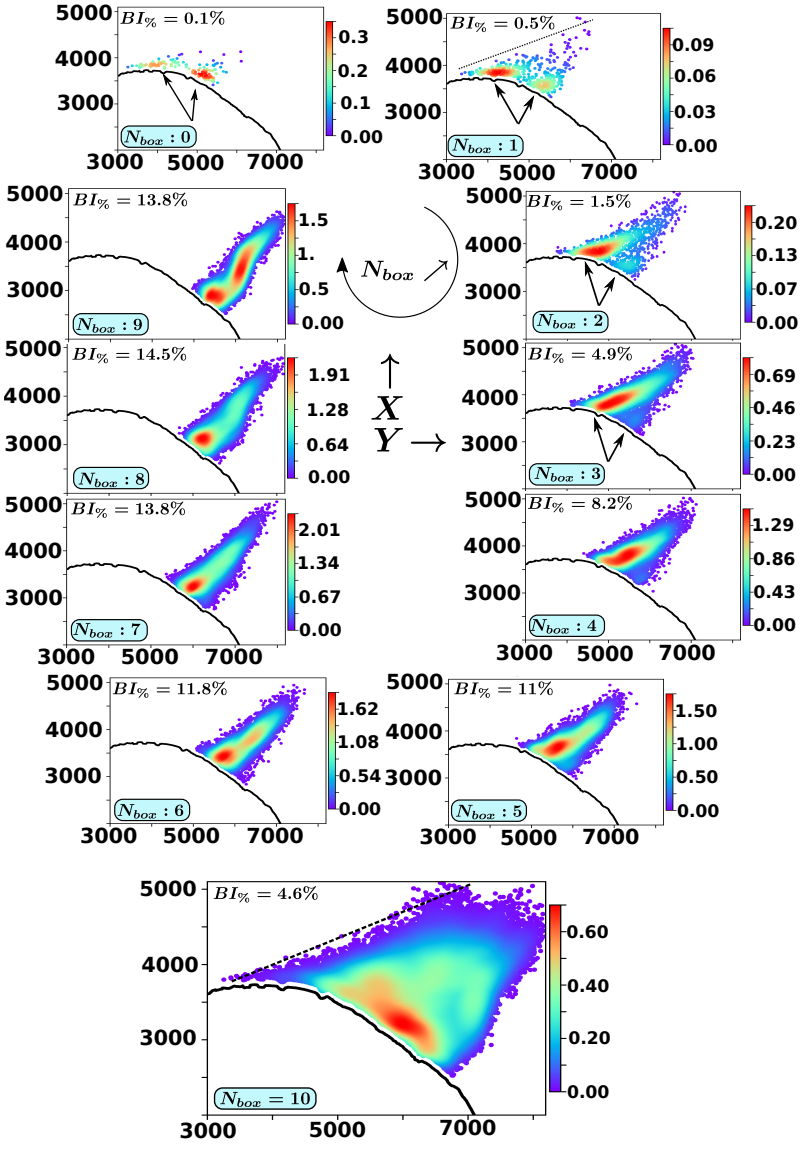

Figure 3. "FCE" configuration: Density of the backstreaming particles within the simulation $X - Y$ plane at the end of the simulation time ($\widetilde{t}_{end} \approx 5.4\widetilde{\tau}_{ci}$ where $\widetilde{\tau}_{ci}$ is the upstream ion cyclotron period). All boxes are plotted from $N_{box} = 0$ with an initial $\theta_{Bn} \approx 90°$ to $N_{box} = 9$ with $\theta_{Bn} \approx 45°$; the bottom panel $N_{box} = 10$ shows aggregate boxes. The color bar represents the spatial distribution of this percentage for each box. The location of the curved shock front is reported (thick black line) at that last time $\widetilde{t}_{end}$. Moreover, we have reported the space integrated percentage value $BI_{\%}$ of backstreaming ions for each box. In order to exclude the gyrating ions present near the front from the backstreaming population, we have eliminated ions being in a small area $\approx 2 - 3\rho_{ci}$ upstream of the shock front; for this reason, a very thin white area is visible along the curved front where no particle is present. The arrows point to the two spots observed at lower N_{box} (see the text for explanations)

.

https://doi.org/10.5194/angeo-2020-9
Preprint. Discussion started: 31 March 2020

Annales Geophysicae Discussions
Open Access
EGU

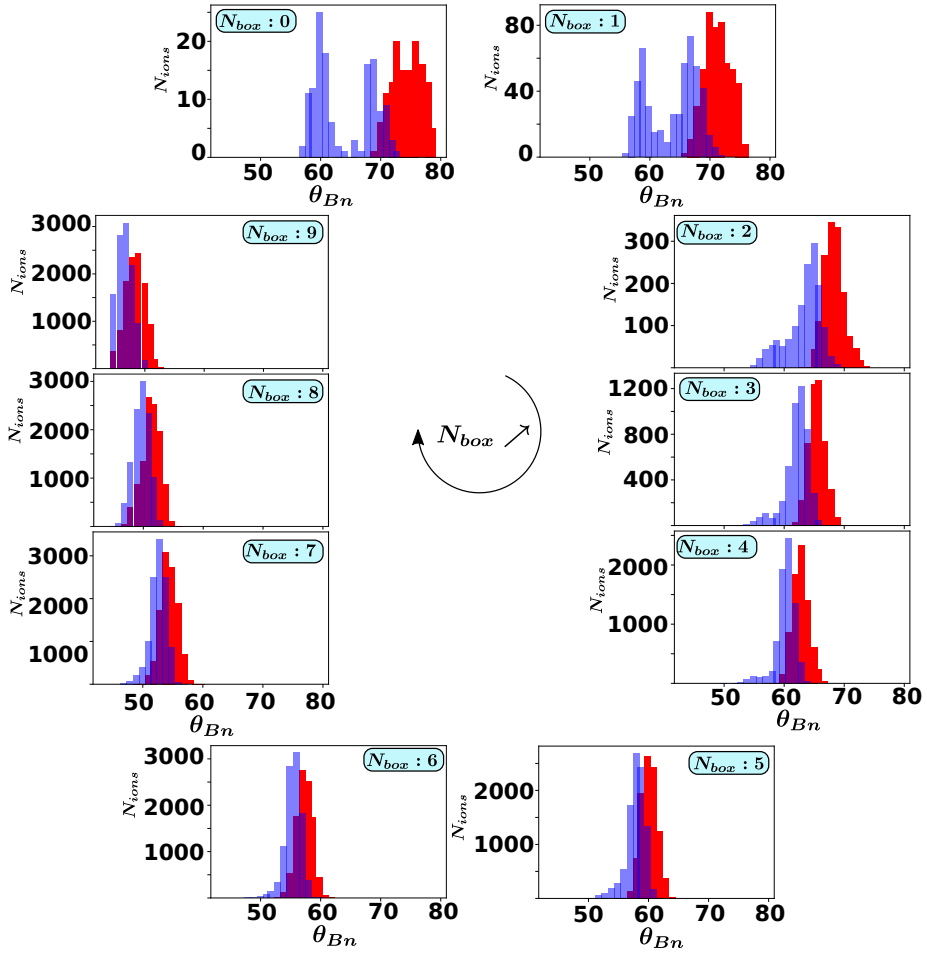

Figure 4. "FCE" configuration: Plots of the ion distribution functions for each $N_{box} = 0 - 9$ versus the local θ_{Bn} angle computed when ions hit for the first time the shock front (red distribution function of the so called θ_{Bn}^{hit}) and when these leave it and escape upstream (blue distribution function versus the so-called θ_{Bn}^{exit}).

consequence, angle values are computed neither at the same time, neither at the same location along the curved front (even if they are located in the same box). In other words, each particle sees different local shock wave profiles in terms of spatial inhomogeneity and time nonstationarity of the shock front. Results are summarized as follows:

First, let us note that the averaged value of θ_{Bn}^{hit} corresponds mainly to the initial location of the box, and therefore, the important feature is not the angle values themselves but rather, the difference between the averaged values of θ_{Bn}^{hit} and θ_{Bn}^{exit} when ions hit and leave the shock front; for this reason, we will use the angular range of particles interaction with the front defined by $\Delta_{int}\theta_{Bn} = \theta_{Bn}^{exit} - \theta_{Bn}^{hit}$. Obviously, θ_{Bn}^{hit} decreases as N_{box} increases until approaching the limit of the quasi-perpendicular domain of propagation i.e. $\theta_{Bn} = 45^o$ for $N_{Box} = 9$.

https://doi.org/10.5194/angeo-2020-9
Preprint. Discussion started: 31 March 2020

Annales Geophysicae Discussions

Second, θ_{Bn}^{hit} reveals to be a good reference entity to be compared with the escaping angle θ_{Bn}^{exit}. Indeed, distribution functions of θ_{Bn}^{exit} strongly differ according to the concerned box. For boxes $N_{Box} = 0-2$, two (blue) peaks occur: one for high θ_{Bn}^{exit} (for which $\Delta_{int}\theta_{Bn} \approx 4-5°$), the other for lower θ_{Bn}^{exit} ($\Delta_{int}\theta_{Bn} \approx 15°$). In terms of time trajectory, the presence of these two peaks suggests that some ions have spent different interaction times (subscript "*int*") within the shock front. Some escape after a short interaction time (i.e. small $\Delta_{int}\theta_{Bn}$) while others escape after a long interaction time (i.e. large $\Delta_{int}\theta_{Bn}$), where the terms short and long refer to a small and large drift along the shock front as already analyzed in Savoini and Lembège (2015). In other words, small drift refers to one bounce whereas large drift refers to multi-bounces process along the shock front.

The range $\Delta_{int}\theta_{Bn}$ can be estimated between the peaks location of both red and blue distributions. More precisely, Figure 4 exhibits one or two peaks in the θ_{Bn}^{exit} distributions according to the N_{box} value. As N_{box} increases (i.e. $N_{box} \geq 3$), the lower θ_{Bn}^{exit} distribution (i.e. correspondingly the largest $\Delta\theta_{Bn}$) decreases rapidly in amplitude and disappears from $N_{Box} = 6$ (i.e. $\theta_{Bn}^{hit} \leq 56^{o}$). Simultaneously, the other peak (i.e. correspondingly the smaller $\Delta_{int}\theta_{Bn}$) becomes dominant for all higher order boxes meaning there are less and less ions associated to large drifts along the shock front.

Third, in order to complete informations deduced from Figure 4, Figure 5 plots the number of reflected ions versus the time spent within the shock front; this interaction time is defined as the time difference between the time associated to θ_{Bn}^{exit} and to θ_{Bn}^{hit}. Different main maxima of backstreaming ions density are evidenced namely f_1, f_2; a third maximum f_3 can be also observed for boxes $N_{box} = 0-4$ but its amplitude is too weak to be relevant in this discussion. One important feature is that f_1 and f_2 appear in all boxes and are independent of the box number. More precisely, f_1 appears about $\Delta\widetilde{T}_{int} \approx 0.25\tau_{ci} \approx \tau_{ci}^{shock}$ while f_2 is observed at $\Delta\widetilde{T}_{int} \approx 1\tau_{ci} \approx 4\tau_{ci}^{shock}$ where τ_{ci}^{shock} is the local gyroperiod estimated within the shock front (at the middle of the ramp). This indicates that the reflection process is not uniform in time but leads to the formation of ion "bursts" associated to the shock dynamics even if the number of ions which spend several gyroperiod τ_{ci}^{shock} within the shock front is rapidly negligible. In addition, for $N_{Box} = 0-2$, f_1 and f_2 have a similar amplitude which is not the case for $N_{Box} = 4-9$. In fact, a close look of f_1 and f_2 shows f_2 does not decrease in magnitude but rather the amplitude of f_1 drastically increases from 10 ($N_{box} = 0$) to 2500 ($N_{box} = 9$). Then, the f_2 population is always present but becomes negligible for lower θ_{Bn} as compared with f_1; this explains why we do not observe two distinct "spots" for $N_{box} = 4-9$.

One helpful aspect of the test particle approach is to include or exclude some electromagnetic field components in order to analyze their impact on the particles dynamics. Indeed, it is clear that some electric field component must be a prerequisite for a large drift along the front (i.e. $\Delta_{int}\theta_{Bn} \approx 15°$) whereas it can not be necessary for the other case $\Delta_{int}\theta_{Bn} \approx 4-5°$. Then, including or not electric field component will shed new light on the origin of backstreaming ions filling the foreshock.

3.2 Impact of electric field components

Savoini and Lembège (2015) have analyzed the impact of $\overrightarrow{E} \times \overrightarrow{B}$ drift on the dynamics of backstreaming ions (Gurgiolo et al., 1983) and, more particularly, as a source of "FAB" and/or "GPB" populations. This study has shown that the origin of both populations can be easily explained in terms of $\overrightarrow{E} \times \overrightarrow{B}$ drift associated or not to a diffusion in the velocity space but was not able to explain the details of the reflection mechanism itself. Then, herein, we will focus on the role of electrostatic field component $\widetilde{E}_l$ within the shock front. The reasons for this particular choice were twofold: $\overrightarrow{E}_l$ has (i) a perpendicular

https://doi.org/10.5194/angeo-2020-9
Preprint. Discussion started: 31 March 2020

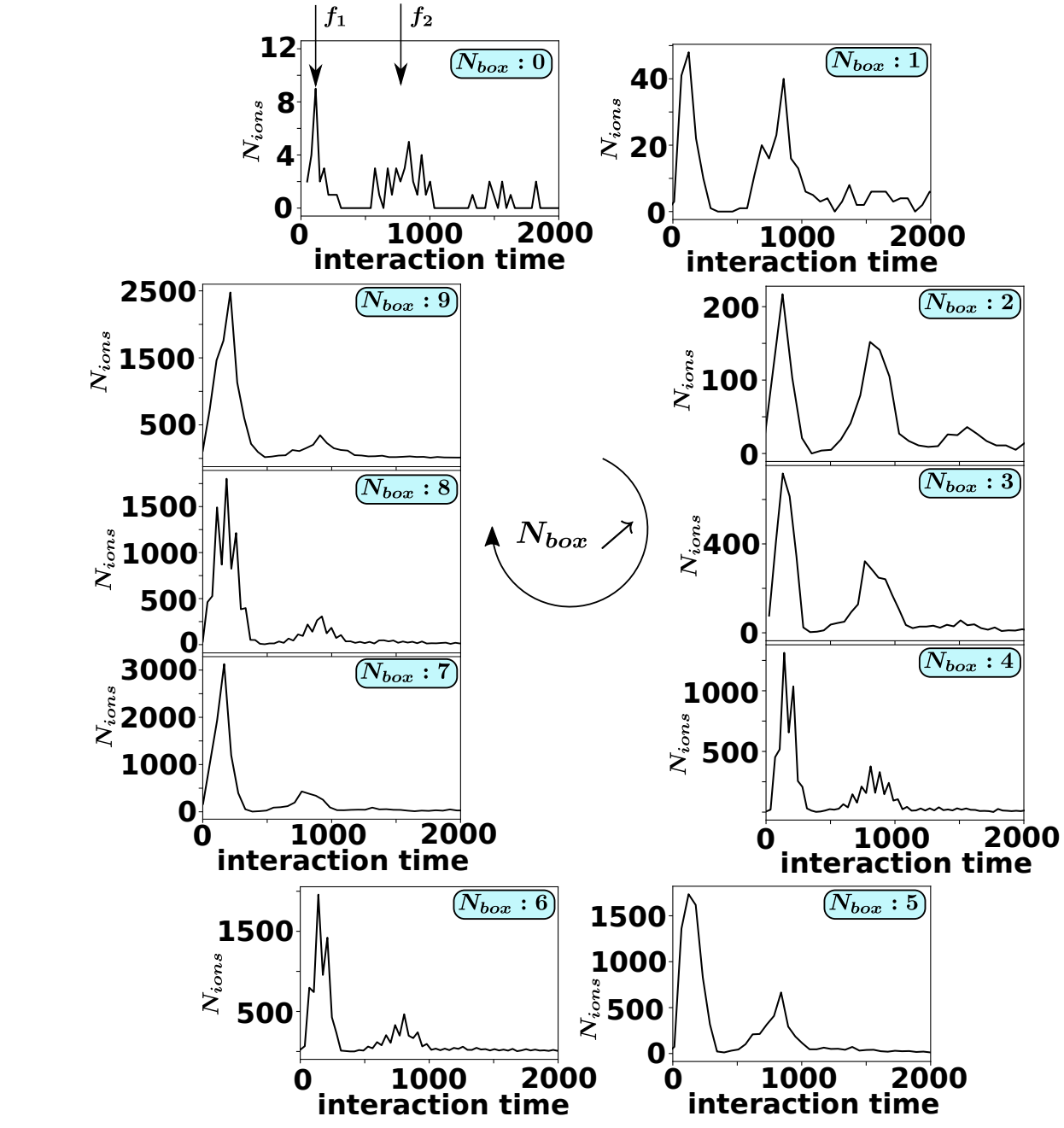

Figure 5. "FCE" configuration: Plots of the ion distribution functions (for each $N_{box} = 0 - 9$) versus the interaction time $\Delta\widetilde{T}_{int}$ spent by each particle within the shock front. As shown, this interaction time is not continuous but evidences distinct "bursts" of reflected ions (hereafter named f_1 and f_2), respectively at $\Delta\widetilde{T}_{int} \approx 0.25\widetilde{\tau}_{ci}$ and $\Delta\widetilde{T}_{int} \approx \widetilde{\tau}_{ci}$, where $\widetilde{\tau}_{ci}$ is the upstream cyclotronic period. A third "burst" of reflected ions can be identified around $\Delta\widetilde{T}_{int} \approx 1.5\widetilde{\tau}_{ci}$ for boxes $N_{Box} = 0 - 2$, but is marginal as compared with the others.

https://doi.org/10.5194/angeo-2020-9
Preprint. Discussion started: 31 March 2020

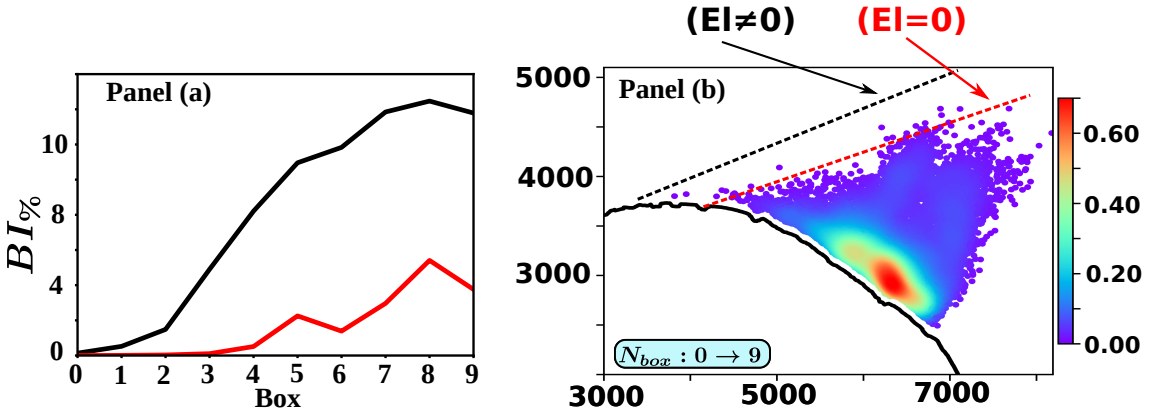

Figure 6. "FCE" configuration: Characteristics of the ion foreshock with and without the electrostatic field component $\widetilde{E}_l$ (i.e. $\widetilde{E}_{lx} = \widetilde{E}_{ly} = 0$). Panel (a) shows the percentage of the backstreaming ions $BI_{\%}$ versus the box number. Black and red curves are defined for $\widetilde{E}_l \neq 0$ and $\widetilde{E}_l = 0$, respectively. Panel (b) shows the density of the backstreaming particles in the same format as Figure 3 but without electric field ($\widetilde{E}_l = 0$). Only the view which aggregates all boxes (i.e. $N_{box} = 10$) is shown in order to evidence the location of the edge of the ion foreshock (dotted line) in each case (in black when $\widetilde{E}_l \neq 0$ and in red when $\widetilde{E}_l = 0$, respectively).

component which can contribute to the $\overrightarrow{E} \times \overrightarrow{B}$ drift and (ii) the parallel component $\overrightarrow{E}_{\parallel}$ can accelerate ions to escape from the shock front. Moreover, the convective electric field $\widetilde{E}_t$ can not be canceled easily since it is induced by the propagating shock wave in the Solar wind reference frame.

Figure 6a shows the percentage $BI_{\%}$ of backstreaming ions versus the box number where the black and red curves are defined for $\widetilde{E}_l \neq 0$ and $\widetilde{E}_l = 0$ respectively. The impact of the $\widetilde{E}_l$ field on the reflection process is clearly apparent for all θ_{Bn} values (namely for all N_{box}). In particular, the percentage $BI_{\%}$ strongly decreases as $\widetilde{E}_l = 0$, which illustrates the dominant role of $\widetilde{E}_l$ field, in particular, for lower box number $N_{Box} = 0 - 3$ (i.e. high θ_{Bn} approaches 90^o) where few backstreaming ions are observed. This point is not surprising if one reminds that for $N_{Box} = 0$ (i.e. largest θ_{Bn}) escaping ions have to be accelerated to higher parallel velocity as reviewed in Burgess et al. (2012) and our simulations reveal that the electric component $\widetilde{E}_{l\parallel}$ is a good candidate to accelerate ions in the parallel direction. Another consequence is illustrated in Figure 6b, which shows that the edge of the ion foreshock is shifted due to the lack of reflected ions and appears around $\theta_{Bn} \approx 55°$. Clearly, the contribution of the electric field is important for ions which populate the edge of the foreshock and need to escape at high θ_{Bn}.

Another way to observe the strong impact of $\widetilde{E}_l$ on the dynamics of reflected ions, is to plot the two θ_{Bn}^{hit} and θ_{Bn}^{exit} distributions in the same format as that of Figure 4. The number of backstreaming ions decreases drastically for all boxes, and is zero for $N_{box} = 0$. Furthermore, the density is not uniform for all boxes and appears to be much more important for $N_{Box} = 5 - 9$ than for $N_{Box} = 1 - 4$. The θ_{Bn}^{exit} distribution is strongly modified and a comparison between Figures 4 and 7 can be summarized as follows:

https://doi.org/10.5194/angeo-2020-9
Preprint. Discussion started: 31 March 2020

Annales Geophysicae Discussions

1. The boxes $N_{Box} = 1-2$ evidence a total absence of reflected ions having a small range $\Delta_{int}\theta_{Bn}$ and only the θ_{Bn}^{exit} distribution around $60°$ persists. This result shows that $\widetilde{E}_l$ plays a key role in the formation of some backstreaming ions and more specifically, for the ions suffering a "one bounce" reflection whereas the ions suffering a large drift (i.e. a $\overrightarrow{E} \times \overrightarrow{B}$ drift) are mainly supported by the $\overrightarrow{E}_t$ induced electric field always included in the simulation due to the propagating shock wave into the Solar wind.

2. As θ_{Bn}^{exit} decreases below $60°$, the distribution in two cases are roughly similar (if one takes into an account the decrease of the backstreaming ion density in Figure 7) which can be interpreted either as the ions have been enough accelerated during their reflection at the shock front or as they need a lower parallel velocity to escape upstream. In both cases, $\overrightarrow{E}_l$ plays a minor role in the reflection process.

3. Then, for lower θ_{Bn} ($N_{Box} = 6-9$), $\widetilde{E}_l$ shows very similar escaping angle distribution between Figure 4 and Figure 7 with a small $\Delta_{int}\theta_{Bn}$. Obviously, for these angles the $\overrightarrow{E}_{l\parallel}$ component is not anymore mandatory and the only reflection process involved can be interpreted as a mirror reflection or Fermi reflection at the shock front.

In summary, the comparison between figures 4 and 7 evidences that $\widetilde{E}_l$ components are essential in the ion reflection for high θ_{Bn}^{exit} angle (i.e. $> 56°$) where ions need strong acceleration process but play a less important role at lower θ_{Bn} angles. Indeed, for $N_{Box} = 6-9$, the reflection process takes place with a small $\Delta_{int}\theta_{Bn}$ with or without the electric field. In other words, the $\overrightarrow{E} \times \overrightarrow{B}$ drift invoked for $\theta_{Bn} \leq 56°$ seems to be mainly supported by the convective electric field components present at the shock front and not by the electrostatic components. Similarly, the "one bounce" reflection always occurs even in absence of $\widetilde{E}_l$ field and then, can be associated to a *Fermi type one acceleration* process which seems to be very efficient especially at lower θ_{Bn}. This "one bounce" reflection (i.e. f_1) is essentially a short time interaction as illustrated in Figure 5 ($\Delta\widetilde{T}_{int} \approx 1\widetilde{\tau}_{ci}^{shock}$)

3.3 Impact of the shock front nonstationarity

Previous studies have largely evidenced that a quasi-perpendicular shock front can be intrinsically non stationnary due to different mechanisms (for a review, see (Lembege et al., 2004; Marcowith et al., 2016)). Then, it is important to analyze the impact of such non stationarity on the temporal ion foreshock dynamics. As a first step, we plot in Figure 8 the time evolution of the backstreaming ions percentage $BI_{\%}$ as these leave the front and escape into the upstream region, where $BI_{\%}$ is the instantaneous rate computed during a time range $\Delta\widetilde{T} = \widetilde{\tau}_{ci}/20$. The time $\widetilde{T}_{init} = 1248$ is the initial time when test-particles are launched into the time-dependent simulation. Results are summarized as follows.

(i) Figure 8 results are obtained as the $\widetilde{E}_l$ field components are included (black curve) and artificially excluded (red curve). Of course, one retrieves that the percentage $BI_{\%}$ strongly decreases as $\widetilde{E}_l$ components are excluded; the impact of $\widetilde{E}_l$ field is emphasized for lower N_{box}. In other words, the backstreaming ions mainly appear for lower θ_{Bn} (i.e. $N_{box} > 5$) even in absence of $\widetilde{E}_l$ field.

ii) Time evolution of the different results may be classified into two groups: (i) a first one concerns boxes $N_{Box} = 0-4$ showing a "slow" increase (almost monotonic) of the reflection rate and (ii) a second group $N_{Box} = 5-9$ which evidences a "steep" increase followed by a "flat-top" shape around $BI_{\%} \approx 1\%$, even if it increases slightly with N_{Box}. At the end of the

https://doi.org/10.5194/angeo-2020-9
Preprint. Discussion started: 31 March 2020

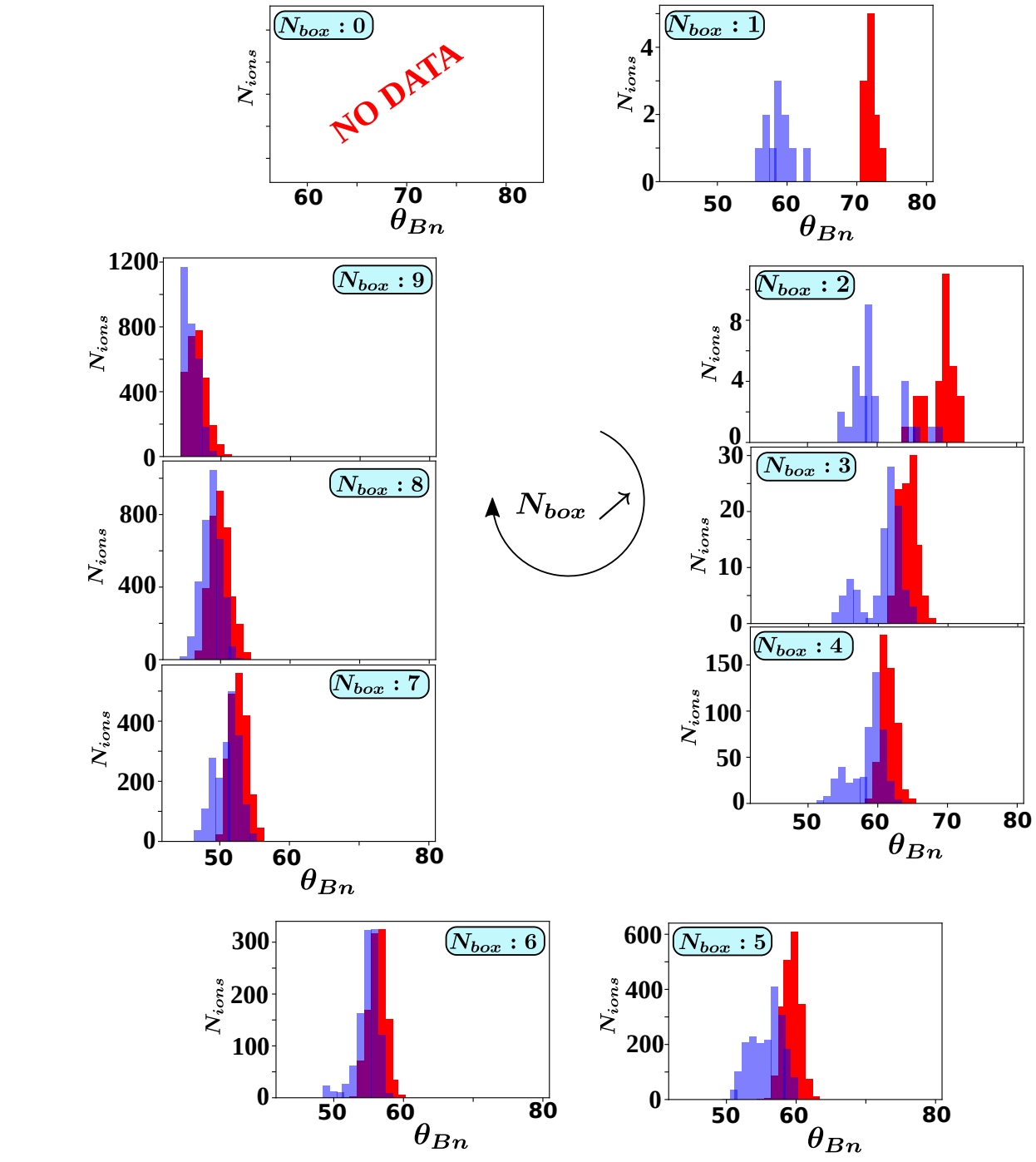

Figure 7. "FCE" configuration: Same plots as for Figure 4 but when electrostatic field components E_{lx} and E_{ly} are artificially excluded

.

https://doi.org/10.5194/angeo-2020-9
Preprint. Discussion started: 31 March 2020

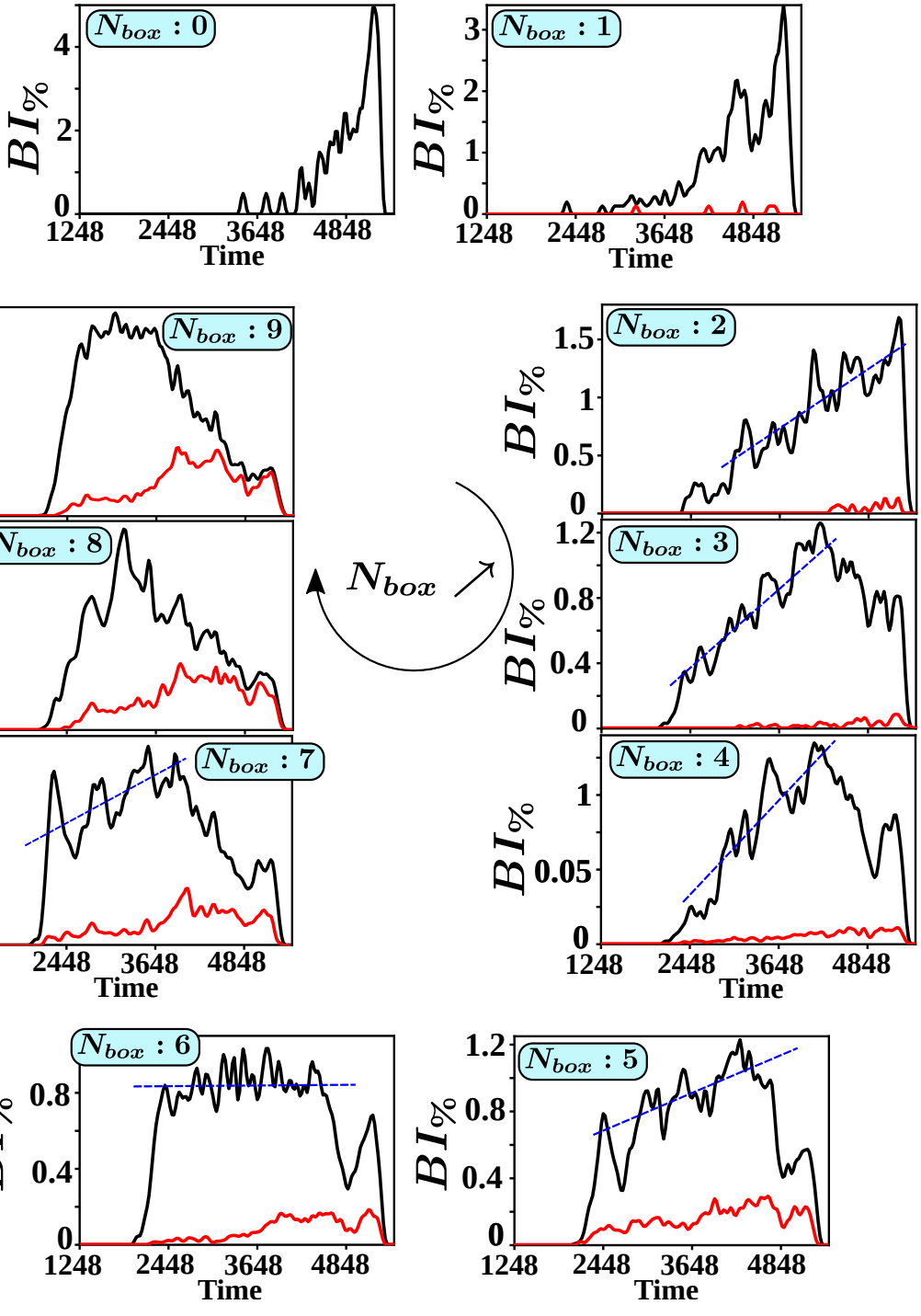

Figure 8. "FCE" configuration: Time history of the reflected ion percentage $BI_{\%}$; each value is computed during a small integrated time interval $\Delta\widetilde{T} = \widetilde{\tau}_{ci}/20$ for the different boxes. Within this interval, only the new reflected ions are memorized. As for the Figure 6, red and blue lines correspond to the case where electric field is included ($\widetilde{E}_l \neq 0$) and excluded ($\widetilde{E}_l = 0$), respectively. We have used the same normalization in order to compare both plots.

https://doi.org/10.5194/angeo-2020-9
Preprint. Discussion started: 31 March 2020


Annales Geophysicae Discussions

simulation, the strong decrease observed for all boxes corresponds to the time when all ions of the different boxes have been swapped by the propagating shock front and then, no more ions are backstreaming.

For the first group, even if all test-particles are initially released at the same distance from the shock front, a delay is observed in the formation of backstreaming ions between the different boxes. For $N_{Box} = 0$, backstreaming ions appear around $\widetilde{T} \approx 4000$ which is about $\approx 2.6\widetilde{\tau}_{ci}$ from the initial release time $\widetilde{T}_{init}$, whereas this time delay decreases to $\widetilde{T} \approx 770$ (i.e. $\widetilde{T} \approx 0.5\widetilde{\tau}_{ci}$) as N_{Box} increases. This illustrates the larger time delay of incoming ions having interacted with the front to escape upstream at high θ_{Bn}. For $N_{Box} = 0-2$, ions have to stay longer within the shock front to finally escape at lower θ_{Bn}^{exit} (Figure 7) which is illustrated by the increase of $BI_{\%}$ as the time evolves (Figure 8). The second group concerns boxes which are already at lower angle θ_{Bn} with easier escaping conditions. In this case, ions are reflected continously with some time variation.

iii) Another interesting feature is the presence of different modulations which are superimposed to a time averaged reflection ion rate (blue dashed line), especially for the boxes $N_{box} = 1-5$ and the boxes $N_{box} = 7-8$. Nearly all boxes exhibit these modulations which represent about 40% of the averaged $BI_{\%}$, even though these modulations amplitude varies versus time and the N_{box}. These evidence a nonstationary ion escaping rate. These modulations almost disappear in the case $\widetilde{E}_l = 0$ (red line).

This result confirms the importance of the electrostatic field component at the shock front in the reflection processes of the backstreaming ions, and most importantly, on the ion foreshock non stationarity behavior as described in previous paper (Savoini and Lembège, 2015).

Nevertheless, it is quite difficult to establish a one-to-one correspondance between these modulations and the non stationarity of the shock front because during the sampling time interval $\Delta\widetilde{T} = \widetilde{\tau}_{ci}/20$ the shock "reformation" and the "time-of-flight" effects have mixed ions coming from either different times and/or different θ_{Bn}^{exit} regions. So this fully self-consistent approach is not totally adapted to resolve this question. A complementary approach is necessary based on simplified simulations with fixed shock front profiles in expansion (nonstationary effects are excluded). This motivates the "**H**omothetic **E**xpansion" model (*HE*") described in the next section.

4 Numerical results: the Homothetic Expansion ("*HE*") model

Figure 9 has been achieved by performing 100 independent simulations. For each simulation, we have followed a propagating "homothetic" shock over a same time range ($\approx 3\tau_{ci}$). During this range, the shock front is "forced" to expand with a dilatation factor proportional to its velocity (see Section 2.2). For example, the chosen time $\widetilde{T} = 4456 \approx 4.2\tau_{ci}$ on the abscissa axis corresponds to one particular shock front profile (i.e. including all electromagnetic field components issued from the previous self-consistent simulation), from which we have measured the instantaneous shock front velocity and that we follow during this large time range covering $\approx 3\tau_{ci}$.

We have selected the 100 last shock profiles of the self-consistent simulation, since these are characteristic of a well developped curved shock with a large curvature radius. The purpose is to determine (i) whether some shock profiles are more

https://doi.org/10.5194/angeo-2020-9
Preprint. Discussion started: 31 March 2020


Annales Geophysicae Discussions Open Access EGU

appropriate than others for the formation of backstreaming ions and (ii) if yes, whether better reflection takes place for some appropriate angular range.

The comparison of Figures 8 and 9 provides the following informations. First, the maximum $BI_{\%}$ value is much higher for the "*HE*" model than for the previous "*FCE*" model for each corresponding box. For example, $BI_{\%}^{max} \approx 1.2$ for $N_{Box} = 9$ in the *FCE* simulations as compared with $BI_{\%}^{max} \approx 15$ in the *HE* configuration. In fact, one has to remind that for *FCE* model the $BI_{\%}^{max}$ value represents an instantaneous reflection rate versus the shock front evolution, whereas this rate is a time integrated value for the *HE* model. Obviously, the main information is not the $BI_{\%}$ value itself but rather its evolution versus time and for different shock profiles. Other main results issued from Figure 9 may be summarized as follows:

1. The $N_{Box} = 0$ box evidences almost no reflection for the majority of the shock front profiles which indicates that the backsteaming ions observed in the *FCE* configuration (i.e. Figure 3) need some specific shock profile related to the shock front nonstationarity in order to escape into the upstream region.

2. Boxes $N_{Box} = 1 - 8$ show clearly some strong modulations in the percentage $BI_{\%}$ versus the shock profile of concern which correspond to a quasi-periodic bursty emission of backstreaming ions. The $BI_{\%}$ rate reaches periodically a maximum value following by a minimum around 0. The corresponding time period $\Delta\widetilde{T}_{max} \approx 460 = 0.5\widetilde{\tau}_{ci}$, is the same for all boxes and correspond to an half gyration within the shock front (i.e. one bounce reflection). The temporal width of each maximum is about $\Delta\widetilde{T}_{range} \approx 256 = 0.25\widetilde{\tau}_{ci}$. These modulations mean that conditions for the emission of backstreaming particles are not intermittent but correspond to some specific shock front profiles. In addition, these modulations appear synchronized in time for the different boxes $1 - 7$ which implies that the local reflection conditions are not strongly dependent of θ_{Bn} angle but rather depend on the shock profile at certain times.

3. In contrast, the boxes $N_{Box} = 8 - 9$ evidence also the same kind of modulations but with greatly reduced amplitude; these are even nonexistent between $\widetilde{T} \approx 3456$ and 4456 which indicates a low sensitivity to the shock front profile when approaching $\theta_{Bn} = 45°$.

4. Similarly, the maximum values $BI_{\%}^{max}$ (black curve) change drastically with box numbers: from small amplitudes $BI_{\%} \leq 6$ for $N_{Box} = 1-2$ (we do not consider the last modulation here) to very high values $BI_{\%} \approx 30$ for $N_{Box} = 3-5$ before decreasing again below 10 for $N_{Box} = 7 - 9$. These variations may be understood by taking account the reflection processes present at these different θ_{Bn} and more specifically, in regards to the electric field component. For boxes $N_{box} = 0 - 2$ reflection is almost impossible without the $\widetilde{E}_{l\|}$ component. As θ_{Bn} decreases (for $N_{box} = 3 - 5$), the reflection becomes easier and both magnetic and electric field contribute to the percentage of reflected ions. Finally, for the last boxes $N_{box} = 6 - 9$, the peaks amplitude decreases but the contribution of $\widetilde{E}_l$ becomes less important in the reflection process as evidenced by comparing both black ($\widetilde{E}_l \neq 0$) and red ($\widetilde{E}_l = 0$) curves. Instead, another process, essentially driven by magnetic field (like fermi type) contributes more since the peaks amplitude of the red curve increases progressively as the box number increases from 6 to 9.

https://doi.org/10.5194/angeo-2020-9
Preprint. Discussion started: 31 March 2020

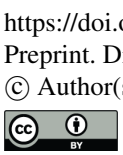

Annales Geophysicae Discussions
Open Access
EGU

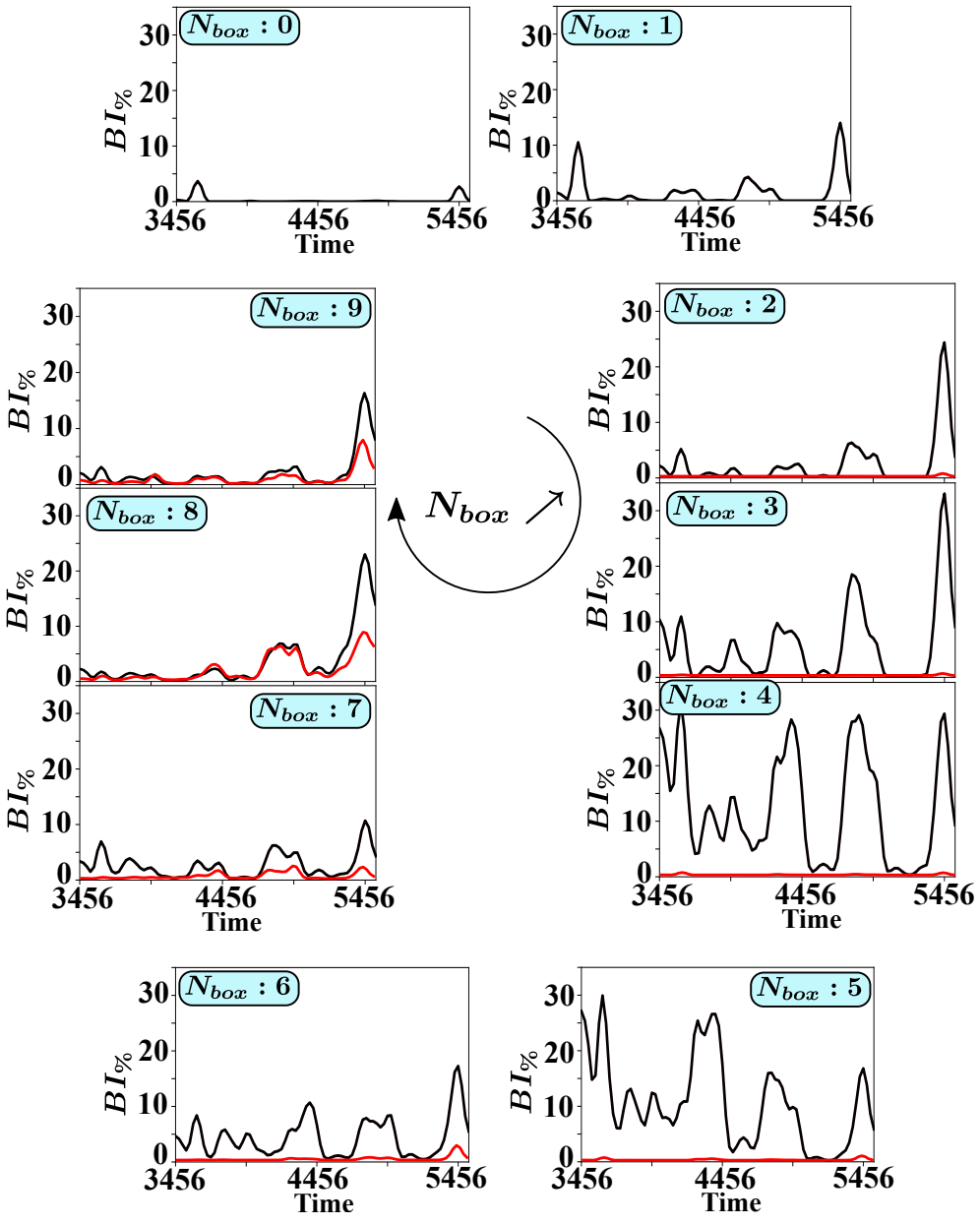

Figure 9. "HE" configuration: Percentage $BI_{\%}$ of backstreaming ions measured at the end of each simulation where each time corresponds to a given fixed shock front. For each shock profile, the simulation covers $10\tau_{ci}$ allowing to obtain a well developped ion foreshock, and $BI_{\%}$ represents the ratio of the backstreaming ions over the total number of upstream ions which are released at the beginning of the simulation. As in Figure 7, black and red lines correspond to the case when E_l field is included and artificially excluded, respectively. The concerned shock profiles are obtained only at late times of the full PIC simulation (from $\widetilde{T} = 3456$ to 5474) where the curvature radius is relatively large ($R > 70\rho_{ci}$).

https://doi.org/10.5194/angeo-2020-9
Preprint. Discussion started: 31 March 2020

Annales Geophysicae Discussions

5. Finally, Figure 9 confirms the key role of E_l field in backstreaming ion formation except when approaching $\theta_{Bn} = 45°$ ($N_{Box} = 8 - 9$) while another reflection process is also at work (in absence of E_l). This represents an indirect way to stress the noticeable impact of Fermi type process related to the magnetic field component in this angular range. This reflection process is more evidenced at lower θ_{Bn} since ions need less parallel velocity to be reflected back into the upstream region. This statement can be quantified more precisely as explained in section 5.

This result is also an illustration to the impact of the electric field built up within the shock front by the different electron-ion dynamics. As well known, this component works to decelerate incoming ions and to accelerate electrons to the downstream region (Savoini and Lemb ege, 1994; Bale et al., 2005). As consequence, this electrostatic component is an essential ingredient in the formation of the backstreaming ions, especially at lower θ_{Bn} where $E_{l\|}$ is higher. Obviously, this is not the case for the electrons which are counteracted in their reflection process by the same parallel component.

5 Discussions

A previous paper (Savoini and Lembège, 2015) has demonstrated that all reflected ions had suffered the same $\overrightarrow{E} \times \overrightarrow{B}$ drift which can account for the pitch angle distribution observed at the shock front. In fact, the key point was the time spent by particles within the front shock which finally decides whether ions will escape to form the "*FAB*" (with a pitch angle $\alpha \approx 0°$) or "*GPB*" populations (with a pitch angle $\alpha \neq 0°$) where α is the angle between the velocity vector and the magnetic field. In other words, the "*FAB*" population may be associated to a large drift along the shock front (and/or long interaction time) during which, particles see a time varying shock front and lose their phase coherency; that correspond to a large angular range $\Delta_{int}\theta_{Bn}$ mentionned in section 3.1. In contrast, the ions of the "*GPB*" population have a shorter interaction time with the shock front associated to a small angular range $\Delta_{int}\theta_{Bn}$.

Unfortunately, self-consistent simulation could not discreminate between the different reflection processes which are involved in the generation of the backstreaming ions. These acceleration processes can be shortly summarized as follows: (i) the "*DSA*" or Diffusive Shock Acceleration (Decker, 1988; Drury, 1999; Sokolov et al., 2006) which involves a particle back and forth between the upstream and the downstream of the shock front, (ii) the "*SDA*" or Shock Drift Acceleration (Webb et al., 1983; Yang et al., 2009) which accelerate ions within the convective electric field present in the shock region and (iii) finally, the "*SSA*" or Shock Surfing Acceleration (Hoshino and Shimada, 2002; Shapiro, 2003; Yang et al., 2009) where the electrostatic field (i.e. electric cross-shock potential) plays a main role in the reflection process (see Marcowith et al. (2016) for a review of these different acceleration processes).

Then, present test-particle simulations allow to have an insight on the origin of the observed "FAB" and "GPB" populations. In particular, these can enlighten the impact of the "*SSA*" on incoming upstream ions by including or excluding the electrostatic field component. Unfortunately, this information is not directly available as we look at the $BI_{\%}$ parameter which evidences only the importance of the electrostatic components on the ion reflection efficiency. Then, we have to analyze more carefully the ion velocity distribution.

https://doi.org/10.5194/angeo-2020-9
Preprint. Discussion started: 31 March 2020

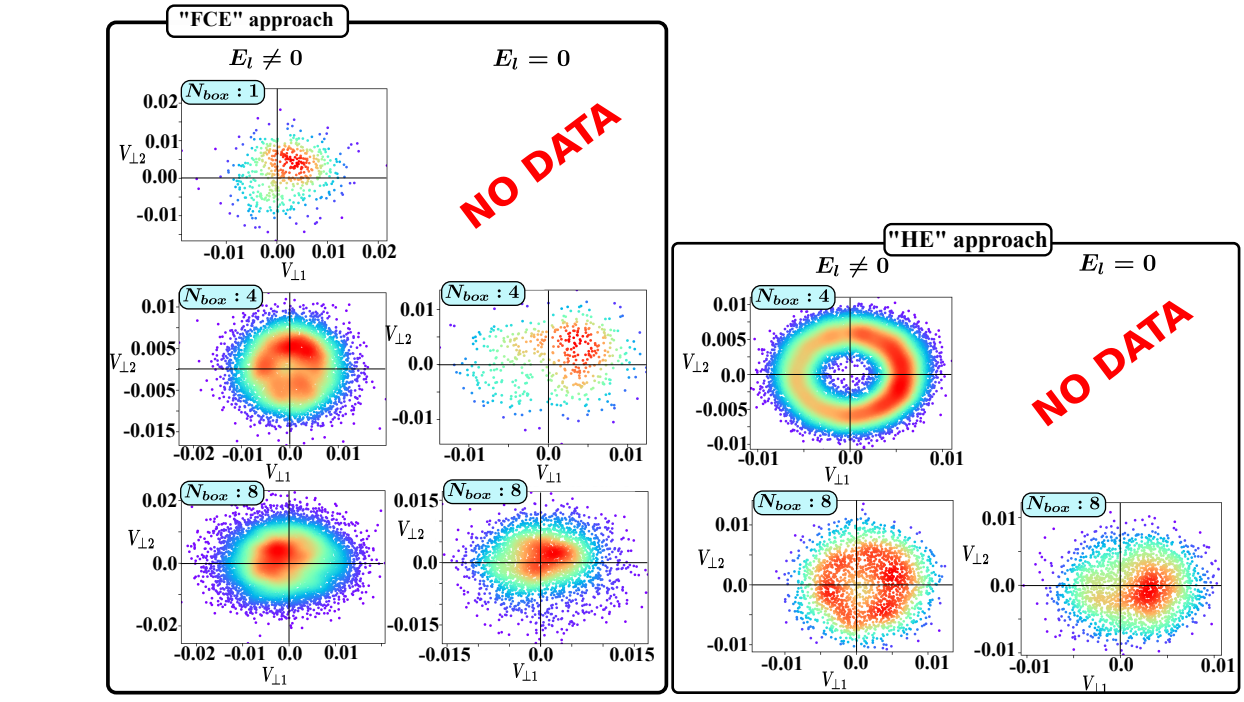

Figure 10. Perpendicular local ion velocity distribution $v_{\perp 1} - v_{\perp 2}$ of all backstreaming ions computed at the end time of the simulations (i.e. after $3\tau_{ci}$ for all simulations) for boxes $N_{Box} = 1, 4$ and 8 in the "*FCE*" approach when the $\widetilde{E}_l$ is included (left panels); the case $\widetilde{E}_l = 0$ is not plotted since the percentage $BI_{\%}$ is very weak (to see Figure 8). The right panels (b) show similar results for the same boxes in "*HE*" configuration in both cases where $\widetilde{E}_l$ is included and excluded; statistical results where $BI_{\%}$ is too weak are not shown. Red and blue colors hold for maximum and minimum value of the distribution function.

Figure 10 plots the local perpendicular velocity distribution functions $f(\overrightarrow{v}_{\perp 1}, \overrightarrow{v}_{\perp 2})$ in both cases (where $\overrightarrow{v}_{\perp 1}$, $\overrightarrow{v}_{\perp 2}$ define the perpendicular velocity components defined with respect to the local magnetic field). All plots are obtained at the end of the simulation; results issued from "*FCE*" (left panels) and "*HE*" (right panels) configurations are considered. Results from three different boxes, $N_{Box} = 1, 4$ and 8, are represented in order to give an overview of the whole ion foreshock components.

Results of the "*FCE*" configuration (left panels) can be analyzed from Figures 4, 7 and 10. Plots of the $E_l \neq 0$ case (Figure 10) show that the $N_{Box} = 1$ evidences approximately a distribution non centered at the $v_{perp} = 0$. Then, particles may be classified as "*GPB*" population with a pitch angle different from 0 (i.e., associated with the smaller $\Delta_{int}\theta_{Bn}$ drift illustrated in Figure 4, peak P_1). Nevertheless, the number of upstream reflected ions is very low which leads to a poor statistic and a noisy $f(\overrightarrow{v}_{\perp 1}, \overrightarrow{v}_{\perp 2})$ distribution. When moving further into the foreshock region (i.e. lower θ_{Bn} angle for $N_{Box} = 4$), the number of reflected ions drastically increase and we observe more clearly the characteristic partial ring of the "*GPB*" population (as in Savoini and Lembège (2015)). In addition, the center of the ring is partially filled-in because of partial diffusion due to particles having large θ_{Bn}^{exit} (i.e., the second spike in Figure 4, peak P_2) and/or by the intrinsic time fluctuations of the front which tends

https://doi.org/10.5194/angeo-2020-9
Preprint. Discussion started: 31 March 2020

Annales Geophysicae Discussions

to blur out the velocity distribution both in perpendicular and parallel directions. At least, in agreement with the associated small θ_{Bn}^{exit} of Figure 4, $N_{Box} = 8$ (in Figure 10) also evidences a non Maxwellian-like distribution ($\alpha \neq 0°$) even if it is much less significant than for $N_{Box} = 4$. When we look the $E_l = 0$ case, we observe roughtly the same behavior for all boxes even if the decrease of the number of backstreaming ions in the box $N_{box} = 8$ makes the comparison difficult.

A further analysis requires a similar approach with the "*HE*" configuration where we follow a succession of independent expanding shock profiles in order to exclude the impact of the time/spatial fluctuations on the diffusion of the velocity distribution $f(\overrightarrow{v}_{\parallel}, \overrightarrow{v}_{\perp})$. Results of the "*HE*" configuration (right panels of Figure 10) show no reflected ions for $N_{Box} = 1$ even with $\widetilde{E}_l \neq 0$ as already emphasized by Figure 9, and for $N_{Box} = 4$ when $\widetilde{E}_l = 0$, so they are not represented in Figure 10. However, $N_{Box} = 4$ exhibits a clear ring which is a feature of the "*GPB*" population; in this case, the center of the ring is not partially filled-in since time velocity diffusion is excluded. These results demonstrate that the formation of the "*FAB*"-like population is also mainly due to the velocity diffusion related to the front time fluctuations which can have different origins as described in previous works (Kucharek et al., 2004; Bale et al., 2005). Finally, for $N_{Box} = 8$, the velocity distribution drastically changes from a ring ($\widetilde{E}_l \neq 0$) to a localized bump ($\widetilde{E}_l = 0$) roughly similar to the case "*FCE*". In both "*FCE*" and "*HE*" approaches, the absence of the electrostatic component leads to a lower ion reflection efficiency (i.e., ions spend longer time within the shock front) and so, to a more diffuse distribution due to space/time front fluctuations.

6 Conclusions

Then, present test-particle simulations reinforce the scenario described in Savoini and Lembège (2015) and have allowed us to investigate more deeply the formation of the backstreaming ions into the foreshock. With this approach, one can evidence more clearly the impact of the shock front non stationarity on the ion foreshock formation and the role of the $\widetilde{E}_l$ electric component on the two kinds of concerned backstreaming populations (i.e. "*GPB*" and "*FAB*" populations). In particular, they have allowed to analyze the dependance of the ion foreshock versus three quantities/effects:(i) the impact of the electrostatic field on the reflection process, (ii) the θ_{Bn} angle, and (iii) the influence of the shock front time/space variations. Results can be summarized as follows (see the synoptic in Figure 11).

1. **Impact of the $\overrightarrow{E}$ field on the ion reflection process**. Both space charge field $\overrightarrow{E}_l$ and convective $\overrightarrow{E}_t$ electric field play an important role in the formation of the backstreaming ions. The $\overrightarrow{E}_l$ component at the shock front increases drastically the percentage of backstreaming ions in the quasi-perpendicular propagation domain as seen in figures 8 and 9. This results was expected as the parallel electric field component $\overrightarrow{E}_{l\parallel}$ accelerates ions towards the upstream region. More precisely, without this electric component, no reflected ions are observed for $\theta_{Bn} > 62°$ whereas in presence of this electric component the edge of the ion foreshock can be established around $\theta_{Bn} > 70°$. In contrast, at lower angles ($\theta_{Bn} \leq 50°$) many ions are reflected without the help of the $\widetilde{E}_l$ component and can be associated to magnetic reflection mechanism (i.e. fast Fermi acceleration). On the other hand, Figure 10 evidences that the convective electric component $\overrightarrow{E}_t$ is always present in our simulation (we are in the solar wind reference frame and then, $\overrightarrow{E}_t \neq 0$ within the propagating shock front) and is responsible for the formation of the "*GPB*"/"*FAB*" populations. Our previous work

https://doi.org/10.5194/angeo-2020-9
Preprint. Discussion started: 31 March 2020

Annales Geophysicae Discussions
Open Access
EGU

(Savoini and Lembège (2015)) was only able to show that the $\overrightarrow{E} \times \overrightarrow{B}$ drift scenario foreseen by Gurgiolo et al. (1983) was at the origin of the two distinct "*FAB*" and "*GPB*" populations but was not able to discreminate between the two distinct component of the electric field. As a conclusion, acceleration of the two populations is mainly supported by the convective electric component and can be associated to the "*SDA*" or Shock Drift Acceleration.

2. **impact of the $\theta_{\mathbf{Bn}}$ angle**. As θ_{Bn} decreases from $90°$ to $45°$, the ion reflection becomes easier since their parallel guiding center velocity needed to overcome the shock front velocity decreases (Paschmann et al., 1980). This behavior is clearly illustrated herein by the increase of the percentage of reflected ions $BI_{\%}$ as θ_{Bn} decreases (i.e., $N_{box} \nearrow$). This behavior persists even in absence of $\overrightarrow{E}_{l\|}$; in this last case, $BI_{\%}$ is only reduced by a factor of 2.5 as illustrated by Figure 6).

3. **Impact of the shock front time/space variations**. Present simulations show that the reflection process is not continuous both in time and in space, but strongly depends on the local shock front profile met by incoming ions at their hitting time. This behavior is difficult to be identified in experimental measurements since the particles coming from different shock locations and at different times are mixed; in contrast, this can be easily evidenced in our "*HE*" test particules configuration. This configuration evidences that particular shock profiles are more suitable for the formation of backstreaming ions than other profiles. Indeed, we observe modulations of the $BI_{\%}$ percentage in Figure 9 which are much more pronounced than in our "*FCE*" configuration. These modulations are so strong that $BI_{\%}$ drops to 0 periodically which means that for certain shock front profiles no ion can escape into the upstream region. This behavior is observed for all N_{box} at the same moment which implies that the ion reflection does not depend on the position along the shock front but essentially on the global profile of the shock at a given time. In the present simulation, we observe 5 distinct "bursts" (i.e. maxima $BI_{\%}$ values) with an average cyclic occurrence period of $1\widetilde{\tau}_{ci}^{shock}$ (where $\widetilde{\tau}_{ci}^{shock}$ is computed at the shock ramp). Surprisingly, $N_{box} = 0$ (Figure 9) does not evidence the same "bursts" as the others, which suggest that the time variations of the shock front are mandatory to obtain backstreaming ions around the edge of the ion foreshock (i.e. high θ_{Bn}).

In summary, present results show that the formation of the ion foreshock is not a continuous process but must be considered as time dependent, which leads to "bursty" emission of backstreaming ions. Three different contributions have been evidenced: (i) a $\overrightarrow{E} \times \overrightarrow{B}$ drift mainly sustained by the convective electric field which is necessary to generate both "*FAB*" and "*GPB*" populations as already emphasized in Savoini and Lembège (2015) and (ii) simultaneously, the contribution of the $\widetilde{E}_l$ component in the ion global reflection process for high θ_{Bn}; (iii) nevertheless, backstreaming ions are still observed within the upstream region even in absence of $\widetilde{E}_l$ for lower θ_{Bn}, which evidences that this population suffers another reflection mechanism which is essentially magnetic in nature such the magnetic mirror reflection.

Unfortunately, the impact of the shock nonstationarity on the ion foreshock is difficult to analyze (see for example Figure 7) for two different reasons: (i) the "*time-of-flight*" effects mix reflected ions coming from different shock profiles (i.e. different reflection times) and (ii) even if some shock profiles are more efficient than others to reflect ions, their respectively impacts disappear rapidly since being blurred out by the impact of less efficient profiles on particles as time evolves.

https://doi.org/10.5194/angeo-2020-9
Preprint. Discussion started: 31 March 2020

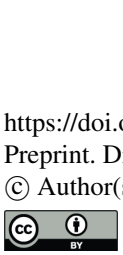

Annales Geophysicae Discussions
Open Access
EGU

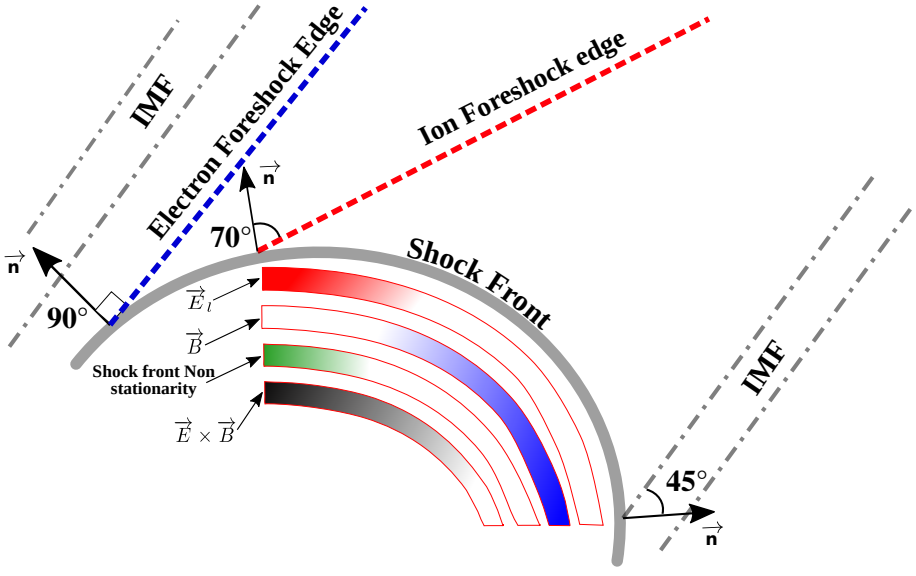

Figure 11. Sketch of the ion foreshock in the quasi perpendicular shock region, illustrating the angular areas along the curved front where the four main identified processes contributing to and/or impacting the formation of backstreaming ions (namely the electric field, the magnetic field, the nonstationary effects and the convection electric field at the shock front). One color (red, blue, green and dark respectively) is associated to each process. The varying strength of the color indicates where the process is strong (full color) or weak (white color). This allows to identify at a glance the angular areas where the different processes are complementary or accumulating one each other. The upstream interplanetary magnetic field (IMF) is reported in grey (dot-dash lines) as well as the box shock itself. Typical angular $\theta_{Bn} = 90^\circ$ and 70° (dot lines in blue and red colors defined between the local shock normal $\boldsymbol{n}$ and the *IMF*) indicates the location where the electron and ion foreshock edge initiates from the curved shock front respectively. The electron foreshock edge is just indicated as a reference.

7 Data availability

435 The data are available at LPP laboratory on the NAS archive

Author contributions. P. Savoini and B. Lembege contributed to the design and implementation of the research, to the analysis of the results and to the writing of the manuscript. The data have been produce by P. Savoini

Competing interests. There is no competing interests for this paper

https://doi.org/10.5194/angeo-2020-9
Preprint. Discussion started: 31 March 2020

Acknowledgements. Numerical simulations were performed on the TGCC computer center located at Bruyeres le Chatel (near Paris), which we thank for its support (DARI project A0050400295). One of the authors (BL) acknowledges the French Centre National d'Etudes Spatiales (CNES) for its support under APR- W-EEXP/10-01-01-05 et APR-Z-ETP-E-0010/01-01-05. This work received financial support by the program "Investissements d'avenir" under the reference ANR-11-IDEX-0004-02 (Plas@Par)

https://doi.org/10.5194/angeo-2020-9
Preprint. Discussion started: 31 March 2020

Annales Geophysicae Discussions
Open Access
EGU

References

Bale, S., Balikhin, M., Horbury, T., and al, e.: Quasi-Perpendicular Shock Structure and Processes, Space Science Reviews, 118, 161–203, https://doi.org/10.1007/s11214-005-3827-0, 2005.

Blanco-Cano, X., Omidi, N., and Russell, C. T.: Global Hybrid Simulations: Foreshock Waves and Cavitons under Radial Interplanetary Magnetic Field Geometry, Journal of Geophysical Research, 114, 01 216, https://doi.org/10.1029/2008JA013406, 2009.

Bonifazi, C. and Moreno, G.: Reflected and Diffuse Ions Backstreaming from the Earth's Bow Shock: 2. Origin, Journal of Geophysical Research, 86, 4405–4413, 1981a.

Bonifazi, C. and Moreno, G.: Reflected and Diffuse Ions Backstreaming from the Earth's Bow Shock. I Basic Properties, Journal of Geophysical Research, 86, 4397–4404, 1981b.

Burgess, D., Möbius, E., and Scholer, M.: Ion Acceleration at the Earth's Bow Shock, Space Science Reviews, 173, 5–47, https://doi.org/10.1007/s11214-012-9901-5, 2012.

Decker, R. B.: The Role of Drifts in Diffusive Shock Acceleration, Astrophys. J., 324, 566, https://doi.org/10.1086/165917, 1988.

Drury, L. O.: An Introduction to the Theory of Diffusive Shock Acceleration of Energetic Particles in Tenuous Plasmas, Reports on Progress in Physics, 46, 973–1027, https://doi.org/10.1088/0034-4885/46/8/002, 1999.

Eastwood, J., Lucek, E., Mazelle, C., and Meziane, K.: The Foreshock, Space Science Reviews, 118, 41–94, https://doi.org/10.1007/s11214-005-3824-3, 2005.

Edmiston, J. P., Kennel, C. F., and Eichler, D.: Escape of Heated Ions Upstream of Quasi-Parallel Shocks, Geophysical Research Letters, 9, 531–534, https://doi.org/10.1029/GL009i005p00531, 1982.

Fuselier, S., Thomsen, M., Gary, S., and Bame, S.: The Phase Relationship between Gyrophase-Bunched Ions and MHD-like Waves, Geophys. Res. Lett., 13, 60–63, 1986a.

Fuselier, S. A.: Ion Distributions in the Earth's Foreshock Upstream from: The Bow Shock, Advance in Space Research, 15, 43–52, 1995.

Fuselier, S. A., Thomsen, M. F., Gosling, J. T., Bame, S. J., and Russell, C. T.: Gyrating and Intermediate Ion Distributions Upstream from the Earth's Bow Shock, Journal of Geophysical Research, 91, 91–99, https://doi.org/10.1029/JA091iA01p00091, 1986b.

Giacalone, J., Jokipii, J. R., and Kota, J.: Ion Injection and Acceleration at Quasi-Perpendicular Shocks, Journal of Geophysical Research, 99, 19–351–19–358, 1994.

Gosling, J. T., Thomsenn, M. F., Bame, S. J., Feldman, W. C., Pashmann, G., and Sckopke, N.: Evidence for Specularly Reflected Ions Upstream from the Quasi-Parallel Bow Shock, Geophys. Res. Lett., 9, 1333–1336, 1982.

Gurgiolo, C., Parks, G. K., and Mauk, B. H.: Upstream Gyrophase Bunched Ions: A Mechanism for Creation at the Bow Shook and the Growth of Velocity Space Structure through Gyrophase Mixing, Journal of Geophysical Research, 88, 9093–9100, https://doi.org/10.1029/JA088iA11p09093, 1983.

Hamza, A. M., Meziane, K., and Mazelle, C.: Oblique Propagation and Nonlinear Wave Particle Processes, Journal of Geophysical Research, 111, 04 104, https://doi.org/10.1029/2005JA011410, 2006.

Hartinger, M. D., Turner, D. L., Plaschke, F., Angelopoulos, V., and Singer, H.: The Role of Transient Ion Foreshock Phenomena in Driving Pc5 ULF Wave Activity, Journal of Geophysical Research, 118, 299–312, https://doi.org/10.1029/2012JA018349, 2013.

Hoshino, M. and Shimada, N.: Nonthermal Electrons at High Mach Number Shocks: Electron Shock Surfing Acceleration, The Astrophysical Journal, 572, 880, https://doi.org/10.1086/340454, 2002.

https://doi.org/10.5194/angeo-2020-9
Preprint. Discussion started: 31 March 2020

Hoshino, M. and Terasawa, T.: Numerical Study of the Upstream Wave Excitation Mechanism. I-Nonlinear Phase Bunching of Beam Ions, Journal of Geophysical Research, 90, 57–64, 1985.

Ipavich, F. M., Galvin, A. B., Gloeckler, G., Scholer, M., and Hovestadt, D.: A Statistical Survey of Ions Observed Upstream of the Earth's Bow Shock - Energy Spectra, Composition, and Spatial Variation, (Upstream Wave and Particle Workshop, 86, 4337–4342, https://doi.org/10.1029/JA086iA06p04337, 1981.

Kempf, Y., Pokhotelov, D., Gutynska, O., Wilson, III, L. B., Walsh, B. M., von Alfthan, S., Hannuksela, O., Sibeck, D. G., and Palmroth, M.: Ion Distributions in the Earth's Foreshock: Hybrid-Vlasov Simulation and THEMIS Observations, Journal of Geophysical Research, 120, 3684–3701, https://doi.org/10.1002/2014JA020519, 2015.

Kucharek, H.: On the Physics of Collisionless Shocks: Cluster Investigations and Simulations, Journal of Atmospheric and Solar-Terrestrial Physics, 70, 316–324, https://doi.org/10.1016/j.jastp.2007.08.052, 2008.

Kucharek, H., Möbius, E., Scholer, M., Mouikis, C., Kistler, L., Horbury, T., Balogh, A., Réme, H., and Bosqued, J.: On the Origin of Field-Aligned Beams at the Quasi-Perpendicular Bow Shock: Multi-Spacecraft Observations by Cluster, Annales Geophysicae, 22, 2301–2308, 2004.

Lembege, B. and Savoini, P.: Nonstationarity of a Two-dimensional Quasiperpendicular Supercritical Collisionless Shock by Self-Reformation, Physic of Fluids, 4, 3533–3548, 1992.

Lembege, B. and Savoini, P.: Formation of Reflected Electron Bursts by the Nonstationarity and Nonuniformity of a Collisionless Shock Front, Journal of Geophysical Research, 107, 1037, https://doi.org/10.1029/2001JA900128, 2002.

Lembege, B., Giacalone, J., Scholer, M., Hada, T., Hoshino, M., Krasnosel'skikh, V., Kucharek, H., Savoini, P., and Terasawa, T.: Selected Problems in Collisionless-Shock Physics, Space Science Reviews, 110, 161–226, https://doi.org/10.1023/B:SPAC.0000023372.12232.b7, 2004.

Marcowith, A., Bret, A., Bykov, A., Dieckman, M. E., Drury, L. O., Lembege, B., Lemoine, M., Morlino, G., Murphy, G., Pelletier, G., Plotnikov, I., Reville, B., Riquelme, M., Sironi, L., and Novo, A. S.: The Microphysics of Collisionless Shock Waves, Reports on Progress in Physics, 79, 046 901, https://doi.org/10.1088/0034-4885/79/4/046901, 2016.

Mazelle, C., Meziane, K., Lequéau, D., Wilber, M., Eastwood, J. P., Rème, H., Sauvaud, J. A., Bosqued, J. M., Dandouras, I., McCarthy, M., Kistler, L. M., Klecker, B., Korth, A., Bavassano-Cattaneo, M. B., Pallocchia, G., Lundin, R., and Balogh, A.: Production of Gyrating Ions from Nonlinear Wave-Particle Interaction Upstream from the Earth's Bow Shock: A Case Study from Cluster-CIS, Planetary and Space Science, 51, 785–795, https://doi.org/10.1016/S0032-0633(03)00107-7, 2003.

Mazelle, C., Meziane, K., and Wilber, M.: Field-Aligned and Gyrating Ion Beams in a Planetary Foreshock, The Physics of \ldots, 781, 89–94, https://doi.org/10.1063/1.2032680, 2005.

Meziane, K.: AIP Conference Proceedings, in: THE PHYSICS OF COLLISIONLESS SHOCKS: 4th Annual IGPP International Astrophysics Conference, pp. 116–122, AIP, https://doi.org/10.1063/1.2032683, 2005.

Möbius, E., Kucharek, H., Mouikis, C., Georgescu, E., Kistler, L. M., Popecki, M. A., Scholer, M., Bosqued, J. M., Rème, H., Carlson, C. W., Klecker, B., Korth, A., Parks, G. K., Sauvaud, J. C., Balsiger, H., Bavassano-Cattaneo, M.-B., Dandouras, I., Dilellis, A. M., Eliasson, L., Formisano, V., Horbury, T., Lennartsson, W., Lundin, R., McCarthy, M., McFadden, J. P., and Paschmann, G.: Observations of the Spatial and Temporal Structure of Field-Aligned Beam and Gyrating Ring Distributions at the Quasi-Perpendicular Bow Shock with Cluster CIS, Annales Geophysicae, 19, 1411, 2001.

Oka, M., Terasawa, T., Saito, Y., and Mukai, T.: Field-Aligned Beam Observations at the Quasi-Perpendicular Bow Shock: Generation and Shock Angle Dependence, Journal of Geophysical Research, 110, 05 101, https://doi.org/10.1029/2004JA010688, 2005.

https://doi.org/10.5194/angeo-2020-9
Preprint. Discussion started: 31 March 2020

Paschmann, G., Sckopke, N., and Asbridge, J.: Energization of Solar Wind Ions by Reflection from the Earth's Bow Shock, Journal of Geophysical Research, 85, 4689–4693, 1980.

Paschmann, G., Sckopke, N., Papamastorakis, I., Asbridge, J. R., Bame, S. J., and Gosling, J. T.: Characteristics of Reflected and Diffuse Ions Upstream from the Earth's Bow Shock, Journal of Geophysical Research, 86, 4355–4364, https://doi.org/10.1029/JA086iA06p04355, 1981.

Savoini, P. and Lemb ege, B.: Electron Dynamics in Two and One Dimensional Oblique Supercritical Collisionless Magnetosonic Shocks, Journal of Geophysical Research, 99, 6609–6635, 1994.

Savoini, P. and Lembège, B.: Two-Dimensional Simulations of a Curved Shock: Self-Consistent Formation of the Electron Foreshock, Journal of Geophysical Research, 106, 12 975, https://doi.org/10.1029/2001JA900007, 2001.

Savoini, P. and Lembège, B.: Production of Nongyrotropic and Gyrotropic Backstreaming Ion Distributions in the Quasi-Perpendicular Ion Foreshock Region, Journal of Geophysical Research, 120, 7154–7171, https://doi.org/10.1002/2015JA021018, 2015.

Savoini, P., Lembege, B., and Stienlet, J.: On the Origin of the Quasi-Perpendicular Ion Foreshock: Full-Particle Simulations, Journal of Geophysical Research, https://doi.org/10.1002/jgra.50158, 2013.

Scholer, M., Fujimoto, M., and Kucharek, H.: Two-Dimensional Simulations of Supercritical Quasi-Parallel Shocks: Upstream Waves, Downstream Waves, and Shock Re-Formation, Journal of Geophysical Research, 98, 18 971–18 984, 1993.

Schwartz, S. J. and Burgess, D.: On the Theoretical/Observational Comparison of Field-Aligned Ion Beams in the Earth's Foreshock, Journal of Geophysical Research, 89, 2381–2384, https://doi.org/10.1029/JA089iA04p02381, 1984.

Schwartz, S. J., Thomsen, M. F., and Gosling, J. T.: Ions Upstream of the Earth's Bow Shock - A Theoretical Comparison of Alternative Source Populations, Journal of Geophysical Research, 88, 2039–2047, https://doi.org/10.1029/JA088iA03p02039, 1983.

Shapiro, V. D.: Shock Surfing Acceleration, Planetary and Space Science, 51, 665–680, https://doi.org/10.1016/S0032-0633(03)00102-8, 2003.

Sokolov, I. V., Roussev, I. I., Fisk, L. A., Lee, M. A., Gombosi, T. I., and Sakai, J. I.: Diffusive Shock Acceleration Theory Revisited, The Astrophysical Journal, 642, L81, https://doi.org/10.1086/504406, 2006.

Sonnerup, B. U. Ö.: Acceleration of Particles Reflected at a Shock Front., Journal of Geophysical Research, 74, 1301–1304, https://doi.org/10.1029/JA074i005p01301, 1969.

Tanaka, M., Goodrich, C. C., Winske, D., and Papadopoulos, K.: A Source of the Backstreaming Ion Beams in the Foreshock Region, Journal of Geophysical Research, 88, 3046–3054, https://doi.org/10.1029/JA088iA04p03046, 1983.

Thomsen, M., Gosling, J., and Bame, S.: Gyrating Ions and Large-Amplitude Monochromatic MHD Waves Upstream of the Earth's Bow Shock, Journal of Geophysical Research, 90, 267–273, 1985.

Thomsen, M. F., Gosling, J. T., and Schwartz, S. J.: Observational Evidence on the Origin of Ions Upstream of the Earth's Bow Shock, Journal of Geophysical Research, 88, 7843–7852, https://doi.org/10.1029/JA088iA10p07843, 1983.

Tsurutani, B. T. and Rodriguez, P.: Upstream Waves and Particles - An Overview of ISEE Results, Journal of Geophysical Research, 86, 4317–4324, 1981.

Turner, D., Angelopoulos, V., Wilson, L., Hietala, H., Omidi, N., and Masters, A.: Particle Acceleration during Interactions between Transient Ion Foreshock Phenomena and Earth's Bow Shock, EGU General Assembly 2014, 16, 2276, 2014.

Webb, G., Axford, W., and Terasawa, T.: On the Drift Mechanism for Energetic Charged Particles at Shocks, The Astrophysical Journal, 1983.

https://doi.org/10.5194/angeo-2020-9
Preprint. Discussion started: 31 March 2020

Yang, Z. W., Lu, Q. M., Lembege, B., and Wang, S.: Shock Front Nonstationarity and Ion Acceleration in Supercritical Perpendicular Shocks,
555 Journal of Geophysical Research, 114, 3111, https://doi.org/10.1029/2008JA013785, 2009.